

Acoustoscillogram: Unlocking Arterial Health Insights via Acoustic Sensing with Low-cost Wired Earphones

XIAOXUAN LIANG*, University of Massachusetts Amherst, USA

ZHAOLONG WEI*, University of Massachusetts Amherst, USA

SHIRUI CAO*, University of Massachusetts Amherst, USA

QUAN ZHANG, University of Massachusetts Amherst, USA

LONGFEI SHANGGUAN, University of Pittsburgh, USA

DONG LI[†], University of Maryland, Baltimore County, USA

JEREMY GUMMESON[†], University of Massachusetts Amherst, USA

Cardiovascular disease is a leading cause of mortality worldwide and a major contributor to rising healthcare costs. Early detection of arterial stiffness through metrics such as Pulse Wave Velocity (PWV) and Augmentation Index (AIx) is essential for cardiovascular disease prevention and treatment. However, conventional measurement methods typically require expensive, specialized equipment and clinical settings. In this paper, we explore the use of everyday earphones to monitor PWV and AIx in daily life by capturing skin displacement waveforms induced by arterial pulsation. However, several key challenges must be addressed. First, detecting subtle skin displacement is difficult due to strong self-interference from the speaker to microphone. To address this, we propose a Doppler shift-based displacement estimation approach to isolate dynamic movements from static interference. Second, estimating PWV requires simultaneous two-point measurements, which is non-trivial with standard earphones. We address this with a hardware-software co-design that connects two earphone pairs via a commercial audio splitter and uses orthogonal frequency division multiplexing (OFDM)-based signal separation to extract displacement signals from both sites. Third, enabling general public use without medical training requires thoughtful system design. To this end, we develop a user-friendly mobile application that provides real-time feedback, along with a 3D-printed enclosure to facilitate ease of use and wide accessibility. We conducted IRB-approved clinical studies with 32 participants, comparing our measurements against ground truths from medical devices. Results show that our method achieves a PWV error of less than 0.5 m/s and an AIx error of less than 4%, meeting established medical standards. Please find the demo of our system [here](#).

CCS Concepts: • Human-centered computing → Mobile devices; • Computer systems organization → Sensor networks.

Additional Key Words and Phrases: Acoustic Sensing, Earphone, Arterial Health, Pulse Wave Velocity, Augmentation Index

ACM Reference Format:

Xiaoxuan Liang, Zhaolong Wei, Shirui Cao, Quan Zhang, Longfei Shangguan, Dong Li, and Jeremy Gummesson. 2025. Acoustoscillogram: Unlocking Arterial Health Insights via Acoustic Sensing with Low-cost Wired Earphones. *Proc. ACM Interact. Mob. Wearable Ubiquitous Technol.* 9, 4, Article 194 (December 2025), 27 pages. <https://doi.org/10.1145/3770690>

*These authors contributed equally to this research.

[†]Co-corresponding author.

Authors' Contact Information: Xiaoxuan Liang, xiaoxuanlian@umass.edu, University of Massachusetts Amherst, Amherst, MA, USA; Zhaolong Wei, xiaoxuanlian@umass.edu, University of Massachusetts Amherst, Amherst, MA, USA; Shirui Cao, shiruicao@umass.edu, University of Massachusetts Amherst, Amherst, MA, USA; Quan Zhang, quanzhang@umass.edu, University of Massachusetts Amherst, Amherst, MA, USA; Longfei Shangguan, longfei@pitt.edu, University of Pittsburgh, Pittsburgh, PA, USA; Dong Li, dli@umbc.edu, University of Maryland, Baltimore County, Baltimore, MD, USA; Jeremy Gummesson, jgummeso@umass.edu, University of Massachusetts Amherst, Amherst, MA, USA.



This work is licensed under a Creative Commons Attribution 4.0 International License.

© 2025 Copyright held by the owner/author(s).

ACM 2474-9567/2025/12-ART194

<https://doi.org/10.1145/3770690>

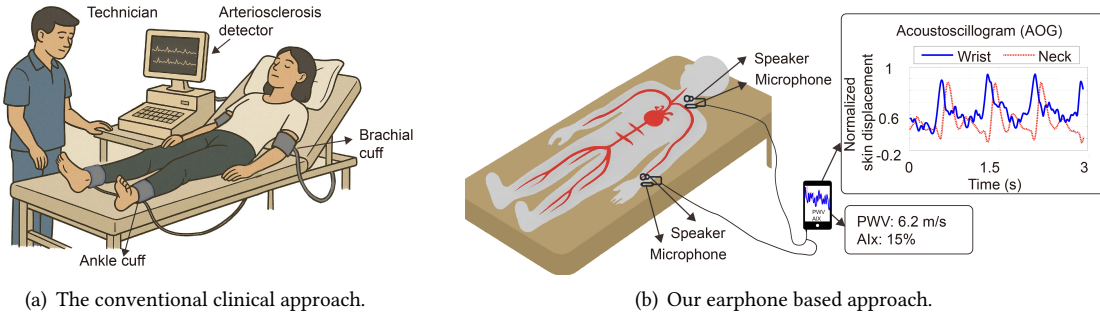


Fig. 1. From clinic to at-home: transitioning from traditional artery stiffness assessment to our innovative earphone-based solution. (a) Conventional clinical methods require trained personnel and specialized equipment to measure PWV and AIx. (b) Our approach enables low-cost, non-invasive arterial health monitoring at home using wired earphones and a smartphone*.

1 INTRODUCTION

Cardiovascular disease (CVD) remains a leading cause of death worldwide, placing immense economic and logistical burdens on national healthcare systems [31, 53]. According to the World Health Organization (WHO) [31, 61], in the U.S. alone, about 30% of adults receive treatment for a cardiovascular condition or risk factor each year, driving an estimated annual cost of nearly \$600 billion. Cardiovascular disease often develops quietly over time, with few noticeable symptoms until a major event such as a heart attack. Yet, as the WHO reports [61, 64], over 80% of premature cardiovascular cases are preventable with early detection and timely treatment.

Evaluating arterial stiffness is a key step in identifying cardiovascular diseases at an early stage. It measures Pulse Wave Velocity (PWV) and Augmentation Index (AIx) [46, 60], two clinically important metrics that serve as early indicators of vascular aging and heightened cardiovascular risk. As shown in Fig. 1(a), PWV is typically derived from two-point measurements that capture the time it takes for a pulse wave generated by the heart to travel between two arterial sites, commonly between the neck (carotid artery), wrist (radial artery), or ankle (posterior tibial artery). AIx, on the other hand, is calculated based on the relative amplitude ratio of the dicrotic notch to the systolic peak in the arterial waveform, typically measured at the wrist.

To date, obtaining accurate measurements of these two metrics requires dedicated clinical equipment such as Atherosclerosis detectors [56], which are costly and not readily available outside of clinical or research environments. Furthermore, these procedures require trained medical personnel to operate the equipment and interpret the results, necessitating in-person hospital or clinic visits. Such logistical and financial constraints make these assessments inaccessible for routine monitoring, particularly in rural areas or underserved communities. As a result, individuals who could benefit most from frequent and long-term cardiovascular monitoring, such as those with hypertension, diabetes, or a family history of cardiovascular diseases, are unable to receive timely assessment and preventive care.

Recent advances in mobile and wearable sensing have enabled the monitoring of various physiological signals using everyday devices, including smartphones, smartwatches, earphones, etc. These signals include heart rate [14], respiratory rate [50], heart sounds [68], and even blood pressure [9, 13, 27], enabling convenient and continuous health monitoring outside of clinical environments. While these measurements offer valuable insights into general cardiovascular status, they only capture the observable effects of vascular conditions rather than directly measuring the underlying mechanical properties of the arterial system. This raises an important question: *can we extend these sensing capabilities to directly estimate arterial health metrics like arterial stiffness, which are*

*This figure is adapted from one originally generated by ChatGPT.

more closely tied to early-stage vascular aging and long-term cardiovascular risk? Answering this question could pave the way for accessible and affordable tools for at-home cardiovascular screening and early intervention.

This paper explores the use of everyday earphones to monitor PWV and AIx. Rather than directly capturing pressure pulse waveforms, our approach reuses earphone as a SONAR system (i.e., speaker as the SONAR transmitter and the line-in microphone as the SONAR receiver) to estimate displacement waveforms generated by subtle tissue oscillations as the pressure pulse wave propagates through the arteries. As illustrated in Fig. 1(b), similar to the clinical setup, we position a pair of earphones at two arterial sites, e.g., one near the neck and the other near the wrist[†]. The earphone's speaker emits acoustic probing signals, which interact with surrounding skin and are modulated by subtle oscillations caused by arterial pulsations during each heartbeat. These signals are reflected and then captured by the earphone' line-in microphone. By analyzing the received signals from both sites, the smartphone visualizes the resulting displacement waveforms in what we term an *Acoustoscillogram* (AOG). From AOG signals, we can estimate pulse transit time and then derive PWV as well as AIx, enabling an accessible and non-invasive solution for continuous arterial health monitoring in everyday settings.

While promising, several challenges must be addressed for real-world deployment. The first challenge lies in estimating subtle displacements induced by tissue oscillations in the presence of strong self-interference. Unlike more noticeable millimeter-level chest movements caused by heartbeat or respiration [2, 37, 50], arterial pulsations in peripheral regions like the wrist and ankle generate much smaller displacements, typically around 0.2 mm [22], making them inherently more difficult to detect. This challenge is further exacerbated in individuals with higher body fat, where increased tissue damping further weakens reflected signals. In addition to signal damping, there exists strong self-interference where acoustic signals propagates directly from the speaker to the microphone without interacting with skin. These interference signals arrive nearly simultaneously with the desired skin reflections but at much higher intensity, masking the subtle displacements we aim to capture.

To address this challenge, we propose estimating skin displacement based on Doppler shifts extracted from the received acoustic signals. The key insight is that, although actual skin displacement is small, Doppler shifts induced by tissue oscillations are relatively large and can be reliably computed due to the high phase resolution of acoustic signals. Moreover, since self-interference signals originate from a static path between the speaker and microphone, they can be effectively distinguished from dynamic reflections associated with tissue oscillations. To extract Doppler shifts, we apply the Hilbert transform to obtain instantaneous phases and compute their time derivative to estimate instantaneous frequencies. These frequency shifts are then used to calculate skin velocities, which are integrated over time to derive displacement waveforms or AOG signals.

The second challenge arises from the requirement of two-point measurement to estimate pulse transit time, which involves placing two pairs of speakers and microphones at separate arterial sites. However, most smartphone audio hardware specifications [12, 17, 51, 57] indicate that, while earphones typically support two output channels for stereo audio playback, the external microphone input is limited to a single recording channel. This hardware limitation makes it difficult to simultaneously record independent reflection signals from two sites.

To address this second challenge, we propose an approach that uses a hardware-software co-design. On the hardware side, we connect two pairs of earphones with a commodity audio splitter [19], each of which consists of two speakers and one microphone. Then the splitter is plugged into the smartphone. Although this setup enables simultaneous recording from two microphones, the recorded signals are mixed into a single input channel on the smartphone. To separate these signals, we introduce a software solution based on orthogonal frequency division multiplexing (OFDM). Specifically, we design the transmitted acoustic signal as a multi-tone waveform, modulating one frequency onto the left audio channel and a different frequency onto the right channel of the splitter. After receiving the mixed signals, they are demodulated to extract the individual frequency components, which are then processed separately to estimate AOG signals from each arterial site.

[†]Our proposed system can also operate at other arterial sites, such as the ankle, as demonstrated in our evaluation.

Table 1. Comparison of our method and prior work for estimating physiological signals, including Respiration Rate (RR), Heart Rate (HR), Heart Rate Variability (HRV), Blood Pressure (BP), Pulse Wave Velocity (PWV), Augmentation Index (AIx).

Technology		Wide availability	Low cost	Low power	Skin tone	Two-point measurement	Measurement location	Physiological signals
IMU	IMU sensor [33]	✓	✓	✓	✓	✗	Chest, Neck	RR, HR
Light	PPG sensor [9, 11, 13, 21, 25, 45, 54]	✗	✓	✓	✗	✓	Finger, Ear canal, etc	HR, BP, PWV
	WiFi device [2]	✗	✗	✗	✓	✗	Chest	RR, HR
RF	RFID device [28, 58]	✗	✗	✗	✓	✗	Chest	RR, HR
	mmWave radar [1, 24, 38]	✗	✗	✗	✓	✗	Wrist, Chest	RR, HR, BP
	Smartphone [50, 65]	✓	✓	✓	✓	✗	Chest	RR, HR
Acoustic	Earphone [15, 20, 67]	✓	✓	✓	✓	✗	Ear canal	RR, HR, HRV
	Our method	✓	✓	✓	✓	✓	Wrist, Neck, Ankle, etc	PWV, AIx

The third challenge is how to enable the system to be easily and reliably used by the general public without the guidance of trained clinicians. First, arteries vary in size, depth, and structure across individuals and body locations, making it non-trivial to accurately locate them. Second, motion artifacts from surrounding muscles can significantly degrade the quality of AOG signals. Third, assembling and positioning speakers and microphones on earphones in a consistent and user-friendly manner remains an open design problem.

To address this third challenge, we develop a mobile application that provides real-time feedback during arterial health measurements. Based on the characteristic physiological patterns in AOG signals, we design a one-dimensional convolutional neural network to assess signal quality and determine whether AOG signals are sufficiently clear for computing PWV and AIx. If no arterial signals are detected due to incorrect positioning or motion artifacts, the application prompts the user to make necessary adjustments. To improve usability and consistency, we also design a 3D-printed enclosure that houses both the speaker and microphone from the standard earphone, and attaches to an adjustable band to ensure stable placement on the body.

The main contributions of this work are summarized as follows:

- To the best of our knowledge, this is the first study to investigate arterial health insights using acoustic sensing with affordable and widely accessible earphones. We believe this system represents a significant step toward enabling at-home arterial risk assessment in real-world settings.
- We propose a series of hardware and software designs to ensure the system operates reliably and is easy to use. These include signal processing algorithms for skin displacement estimation, signal modulation and demodulation techniques for simultaneous sensing at two arterial sites, sensor designs featuring 3D-printed enclosures, and a mobile application that guides users through the measurement process.
- We implement our prototype real-time system and test it on various devices, including 6 smartphones and 6 earphones. Our results demonstrate the feasibility of using widely available wired earphones for arterial health monitoring. Please find the demo of our arterial health monitoring system [here](#).
- We conducted extensive clinical experiments with 32 human subjects under IRB-approved protocols, including 26 healthy individuals and 6 patients with cardiovascular conditions. We compared our estimated PWV and AIx values against ground truth measurements obtained from clinical-grade devices. The results demonstrate high accuracy, with a mean absolute error of less than 0.5 m/s for PWV and less than 4% for AIx, meeting established medical standards[‡] [10, 26, 34, 44, 49, 52].

[‡]According to clinical guidelines, PWV measurement methods typically exhibit a bias of less than 1 m/s when validated against gold-standard references [10, 34]. For AIx, invasive and tonometry-based methods generally show a bias of 4–12% [10, 26, 44, 49, 52]. In alignment with these standards, we conservatively adopt a 4% threshold as an acceptable error margin.

2 RELATED WORK

In this section, we review prior studies on physiological signal monitoring using various sensing technologies in mobile and wearable devices, while highlighting how our approach to arterial health monitoring differs from existing methods. As summarized in Table 1, these technologies are categorized based on the types of signals they utilize, including inertial measurement units (IMU), light, radio frequency (RF), pressure, and acoustic signals.

IMU sensors offer a low-cost, low-power solution for physiological monitoring and are commonly integrated into mobile and wearable devices. When placed on the neck or chest, they can enable respiration rate and heart rate monitoring without optical or electrical contact [33]. However, even minor body movements can introduce significant noise and reduce accuracy [43]. Moreover, IMUs are generally limited to basic metrics and lack the sensitivity required for estimating advanced cardiovascular parameters [43].

Light-based methods, particularly those using photoplethysmography (PPG) sensors, are among the most widely adopted techniques for physiological signal monitoring [6, 9, 13, 21]. Commodity smartwatches commonly use PPG to track heart rate. Beyond this, several systems estimate blood pressure using PPG signals by capturing pulse transit time or blood volume changes. For example, Crisp-BP [13] monitors blood vessel volume over the cardiac cycle, while other approaches use ear canal pressure variations [9] or head-mounted light intensity changes [25]. Stereo-BP [6] estimates blood pressure by measuring the pulse time difference between PPG signals from left and right ear-worn devices. In addition, Byfield et al. [11] introduced a dual-PPG sensor system that estimates PWV by tracking pulse arrival times between the fingertip and knuckle. Despite their popularity, light-based methods have notable limitations. They are highly sensitive to skin tone, with signal quality often degrading in individuals with darker skin [32]. Although MacIsaac et al. [42] and Guo et al. [23] have proposed optimization techniques to mitigate this issue, these approaches typically require additional hardware or complex algorithms, which may limit their practicality in real-world applications.

Recent studies have explored the use of wireless signals such as WiFi, RFID, and mmWave for physiological monitoring [2, 39, 58]. While these methods are device-free and capable of capturing respiration and heart rate, they suffer from key limitations. For example, Adib et al. [2] used a customized WiFi setup, making it impractical for widespread or consumer use. RFID systems face similar cost and complexity barriers [58], and both WiFi and RFID lack the spatial resolution necessary to detect advanced cardiovascular parameters. Although mmWave technology offers higher resolution [39], its modules are still expensive (around \$200) and consume significant power, limiting their suitability for low-cost, continuous, or large-scale deployment.

More recently, researchers have explored the use of acoustic signals captured by earphones to monitor physiological parameters. APG [20] enables robust cardiac monitoring using mass-market active noise cancellation (ANC) headphones. HearBP [67] estimates blood pressure using in-ear microphones based on heart sounds. Asclepius [15] introduces a low-cost plug-in peripheral that repurposes an earphone's speaker as a microphone to capture subtle phonocardiogram (PCG) signals from the ear canal. However, these systems rely on expensive ANC headphones, earphones with built-in in-ear microphones, or customized hardware. In contrast, our system uses low-cost wired earphones and focuses on arterial health insights, such as PWV and AIx, rather than general cardiovascular metrics like heart rate, heart rate variability, or heart sounds.

To address the limitations of existing work, our approach re-purposes earphones as a SONAR system to estimate displacement waveforms generated by subtle tissue oscillations as the arterial pulse wave propagates through the body. By leveraging built-in speakers and microphones, the system emits acoustic signals and analyzes the reflected waves to detect synchronized skin movements at multiple arterial sites. This enables the estimation of advanced cardiovascular metrics such as PWV and AIx in a low-cost, portable, and widely accessible manner.

3 The Basics of PWV AND AIx MEASUREMENT

This section describes the basics of calculating Pulse Wave Velocity (PWV) and Augmentation Index (AIx) [46].

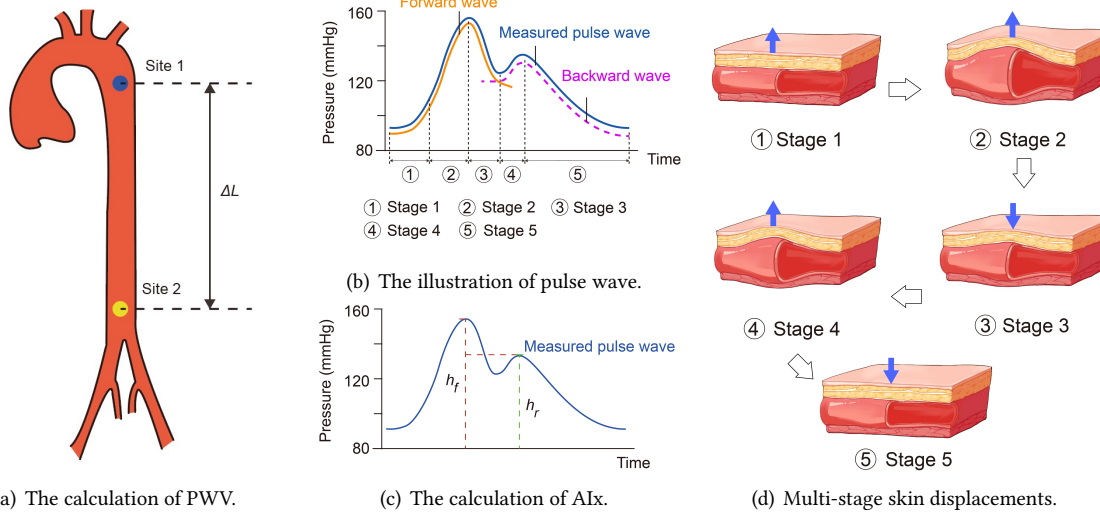


Fig. 2. The illustration of PWV and AIx measurement, pulse wave dynamics, and skin displacement. (a) shows the two-point measurement setup for PWV, where ΔL is the distance between two arterial sites. (b) illustrates the pulse waveform, including the forward and backward wave components, and (c) shows how AIx is calculated from the waveform peaks. (d) depicts the multi-stage skin displacements that occur during one cardiac cycle, corresponding to the wave propagation stages.

3.1 Calculating PWV

As shown in Fig. 2(a), PWV is clinically defined as the speed at which pressure waves, generated by the heart during systolic ejection, propagate along the arterial walls. It is calculated as:

$$\text{PWV} = \frac{\Delta L}{\Delta t}, \quad (1)$$

where ΔL is the distance between two arterial sites (Site 1 and Site 2), which is obtained using tape measures to measure the surface (epidermal) distance along the body. Δt represents the Pulse Wave Transit Time (PWTT), defined as the time delay between the arrival of the same wavefront of the pulse pressure wave at the two sites.

PWV is a widely recognized indicator of arterial stiffness [46], as its value is directly influenced by the elasticity of the vascular walls and positively correlated with the degree of arteriosclerosis. For example, a healthy PWV measured between the neck and wrist typically falls within the range of 4–8 m/s [7, 62]. Values exceeding this range suggest reduced arterial elasticity and are associated with an elevated risk of cardiovascular disease [5, 46]. An elevated PWV is primarily indicative of increased arterial stiffness when assessed through repeated measurements within the same individual [46, 60, 62]. Due to its reliability and repeatability, PWV is considered the “gold standard” for non-invasive assessment of arterial stiffness [46, 60].

3.2 Calculating AIx

As illustrated in Fig. 2(c), AIx is clinically defined as the ratio between the amplitude of the backward wave and the forward wave in a single cardiac cycle:

$$\text{AIx} = \frac{h_r}{h_f} \times 100\%, \quad (2)$$

where h_r and h_f are the peak heights of the backward and forward waves, respectively, within the same cycle.

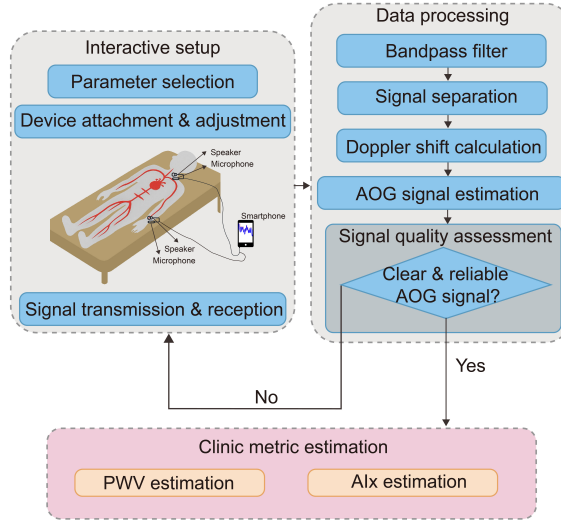


Fig. 3. Overview of our proposed system.

AIx is a non-invasive marker of arterial stiffness and wave reflection with strong clinical relevance. It reflects arterial function and predicts cardiovascular events. Higher AIx indicates stiffer arteries, stronger backward waves, and greater cardiac load [8, 44]. In healthy individuals aged 20–30, AIx typically remains below 15%. Chronically elevated AIx may increase cardiac workload and harm organs like the kidneys [55]. Additionally, AIx is sensitive to changes in vascular elasticity and can more effectively reflect pharmacological effects than blood pressure or PWV, thereby supporting clinicians in optimizing therapeutic strategies [8].

4 UNDERSTANDING PRESSURE PULSES AND SKIN DISPLACEMENT

As illustrated in Fig. 2(a), pulse waves are generated by the heart and propagate through the arterial system. During each cardiac cycle, the heart contracts, opening the aortic valve and allowing blood to flow from the left ventricle into the aorta. As the resulting forward wave travels along the arterial walls, it encounters anatomical features such as vascular bifurcations, which reflect part of the wave and produce a backward wave. The pressure pulse waveform is thus formed by the superposition of these forward and backward waves, as depicted in Fig. 2(b). In clinical settings, these waveforms are typically measured using Atherosclerosis detectors or oscillometric cuffs, which detect pressure changes at specific arterial sites such as the carotid or radial artery.

From Pressure Pulse Waveform to skin displacement Waveform. Given the elastic nature of blood vessels [16], the vascular wall expands and contracts in response to changing flow dynamics during the cardiac cycle. This leads to continuous variations in vessel diameter and volume. Because most arteries are located superficially, around 10 mm beneath the skin [18, 40], and are surrounded by soft, elastic tissues, the mechanical force from arterial wall motion is transmitted to the surrounding tissues, inducing their displacement [40].

Fig. 2(d) further emulates skin displacements at various stages of the pressure pulse waveform shown in Fig. 2(b). (i) *Stage 1 to Stage 2:* When the heart contracts and ejects blood, the resulting forward wave rapidly dilates the vessel wall at the measurement site. This dilation pushes the overlying tissues outward, producing an upward displacement. (ii) *Stage 2 to Stage 3:* As the forward wave passes, the vessel gradually returns to its resting state, and the surrounding tissue undergoes downward displacement due to elastic recoil. (iii) *Stage 3 to Stage 4:* When the backward wave reaches the same site, it induces another, smaller dilation of the vessel wall,

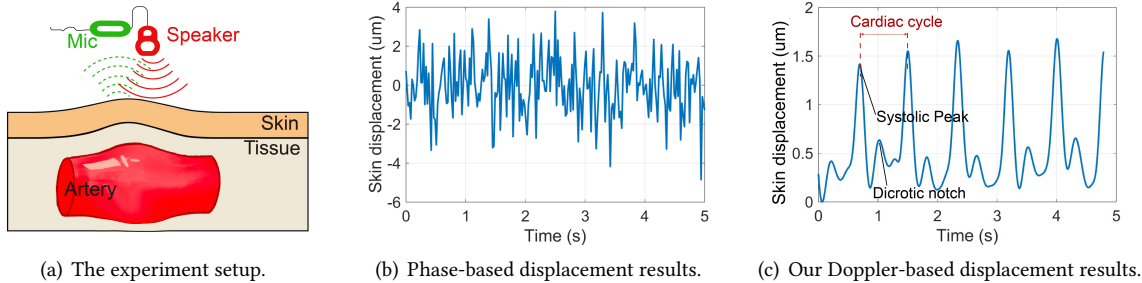


Fig. 4. Comparison between phase-based vs our Doppler-based displacement estimation. (a) Experiment setup showing the speaker and microphone positioned above the skin surface to sense displacement caused by underlying tissue oscillation. (b) Displacement estimated using the phase-based method, showing noisy and non-periodic patterns. (c) Displacement estimated using our Doppler-based method, revealing clean, periodic waveforms synchronized with cardiac cycles.

resulting in a weaker upward displacement of the tissue. (iv) *Stage 4 to Stage 5*: As the backward wave dissipates, the tissue returns to its baseline position, completing the cycle and preparing for the next cardiac event.

This sequence of displacements forms an oscillatory tissue motion pattern that is synchronized with the cardiac cycle. Rather than directly measuring pressure waveforms, our approach repurposes earphones as a SONAR system to estimate displacement waveforms generated by subtle tissue oscillations as the pulse wave propagates through the arteries. These displacement signals are captured and visualized as Acoustoscillogram (AOG) signals, which reflect the mechanical response of tissue to the underlying arterial pressure wave.

5 Our Approach

5.1 System Overview

Fig. 3 presents an overview of our system, which enables non-invasive arterial health monitoring using commodity earphones with a mobile device. The system consists of three main stages: interactive setup, data processing, and clinical metric estimation. In the interactive setup stage, users begin by selecting measurement parameters such as transmission frequency. They then attach and adjust the sensing devices (earphones) at two arterial sites, e.g., the neck and wrist, following in-app guidance. Once the setup is complete, the mobile application emits the acoustic signal and receives the reflected signal to initiate data collection. During the data processing stage, the collected audio signals undergo several steps. A bandpass filter removes unwanted frequency components, followed by signal separation based on Orthogonal Frequency Division Multiplexing. Doppler shifts are then calculated from the reflected signals, which are used to estimate the AOG signals. Then a lightweight neural network performs a real-time signal quality assessment. If the signal is confirmed to be a clear and reliable AOG signal, the system proceeds to the final stage. Otherwise, users are prompted to adjust the device placement and repeat the process. In the final clinical metric estimation stage, the system computes PWV and AIx using the estimated AOG signals. These metrics are then displayed in the app interface, offering users an accessible and affordable method for continuous cardiovascular monitoring.

5.2 Estimating AOG Signals

In this section, we present how we estimate subtle skin displacements induced by tissue oscillations, i.e., AOG signals, in the presence of strong self-interference.

5.2.1 Acoustic Sensing Principle. Continuous wave signals are widely adopted for extracting subtle displacements in acoustic sensing systems due to its simplicity and ability to preserve phase information [59]. As shown in

Fig. 4(a), the earphone’s speaker continuously emits single-tone sinusoidal signals, which can be denoted as:

$$s(t) = A \cos(2\pi f t), \quad (3)$$

where A represents the amplitude, and f denotes the frequency of the transmitted acoustic signals. The signals reflect from the skin and are then captured by the microphone. By analyzing the reflected signals, we can extract fine-grained displacement information caused by tissue oscillations.

5.2.2 Limitations in Prior Studies. To estimate displacement from subtle movements, prior studies [59, 66] adopt a phase-based method that leverages the coherent nature of acoustic signals transmitted and received by the same device. These systems down-convert received signals to a complex baseband using a coherent detector and tracks phase variations over time, which correspond to changes in path length between the moving target and the device. However, as illustrated in Fig. 4(b), this approach is susceptible to strong self-interference, i.e., signals that travel directly from the speaker to the microphone without interacting with skin. These direct-path signals arrive nearly simultaneously with the weaker skin reflections but at significantly higher intensity, effectively masking the subtle displacements that the system aims to detect.

5.2.3 Doppler shift-based Displacement Estimation. Instead of directly calculating displacement from phase values, we estimate skin displacement by first extracting the Doppler shift and then deriving velocity and displacement. The key insight is that, since there is no relative motion between the speaker and microphone, the self-interference signal traveling directly through air does not induce any Doppler shift. This characteristic enables the separation of static self-interference from dynamic reflections caused by tissue oscillations, thereby improving the robustness and accuracy of displacement estimation.

The Doppler shift refers to the change in frequency of a received signal caused by the relative motion between the acoustic device and the reflecting surface [36, 38]. Suppose that the Doppler shift caused by tissue oscillation is f_d , the received signal can be modeled as:

$$s'(t) = A' \cos(2\pi f t + \phi(t)), \quad (4)$$

where A' is the attenuated amplitude, and $\phi(t) = 2\pi f_d t$ is a time-varying phase component due to motion. To compute the Doppler shift f_d , we apply the Hilbert transform to obtain the orthogonal (imaginary) component of the original reflect signal $\hat{s}'(t)$. Then we compute the instantaneous phase $\phi'(t)$ of the received signals as:

$$\phi'(t) = \tan^{-1} \left(\frac{\hat{s}'(t)}{s'(t)} \right). \quad (5)$$

Due to the periodic nature of the arctangent function, the resulting phase may exhibit abrupt 2π discontinuities, which is commonly referred to as phase wrapping. These discontinuities can introduce spurious high-frequency components when directly differentiating the wrapped phase to compute the instantaneous frequency. To address this, we apply phase unwrapping, which adjusts the phase by adding or subtracting 2π whenever a jump greater than π is detected, thereby ensuring a smooth and continuous phase trajectory over time. Finally, the instantaneous frequency $f''(t)$ is obtained by differentiating the unwrapped phase with respect to time:

$$f''(t) = \frac{1}{2\pi} \cdot \frac{d\phi'(t)}{dt}, \quad (6)$$

The Doppler shift is computed as the deviation from the original carrier frequency f , given by $f'_d(t) = f''(t) - f$. To isolate the relevant heart-induced motion, we apply a low-pass filter to $f'_d(t)$, focusing on components typically below 5 Hz. Then the instantaneous velocity $v'(t)$ of skin surface is computed as:

$$v'(t) = \frac{f'_d(t) \times c}{2f} \quad (7)$$

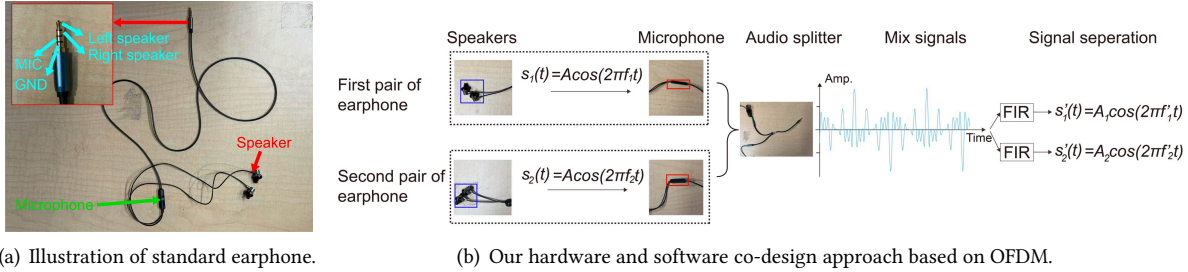


Fig. 5. Signal processing using dual earphone setup. (a) Hardware setup showing a standard earphone pair with stereo speakers and a microphone. (b) Each speaker transmits a unique frequency (f_1, f_2). Reflections are captured and mixed via an audio splitter. Band-pass FIR filters are then applied to separate signals from the two arterial sites.

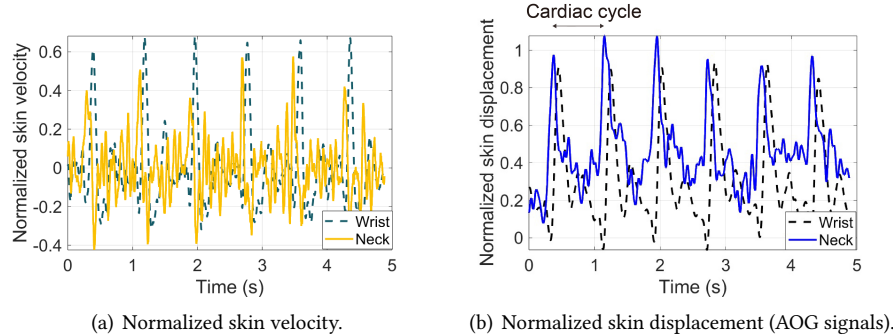


Fig. 6. The sensing results at two arterial sites, i.e., wrist and neck.

where c is the speed of sound in air (approximately 343 m/s), and the factor of 2 accounts for the round-trip propagation between the device and the reflecting surface. To obtain a more reliable representation of tissue oscillation, we consider displacement over an entire cardiac cycle as a more robust metric. After obtaining the instantaneous velocity, the displacement $r(t)$ at time t is computed by integrating the velocity over time:

$$r(t) = \int_{t_0}^t v'(\tau) d\tau, \quad (8)$$

where t_0 denotes the initial time, and $v'(\tau)$ represents the instantaneous velocity at time τ . As shown in Fig. 4(c), our method clearly captures skin displacement induced by underlying tissue oscillations, producing a clean and periodic waveform aligned with cardiac cycles, and demonstrating improved signal clarity and robustness.

5.3 Enabling Two-point Measurements

To compute PWV, AOG signals must be collected from two arterial sites, such as the neck and wrist, by placing separate pairs of speakers and microphones at each location. However, as illustrated in Fig. 5(a), the standard 3.5mm TRRS (Tip-Ring-Ring-Sleeve) audio jack configuration used in commodity earphones presents a key limitation. In this configuration, the tip and first ring are used for left and right audio output, the second ring serves as a shared ground, and the sleeve is dedicated to a single line-in microphone input. As a result, most earphones support only one microphone channel, making it infeasible to simultaneously record independent acoustic reflections from two sites using a single pair of earphones.

To address this limitation, we propose a hardware-software co-design approach. On the hardware side, as illustrated in Fig. 5(b), we connect two pairs of earphones to a commodity audio splitter [19], where each pair

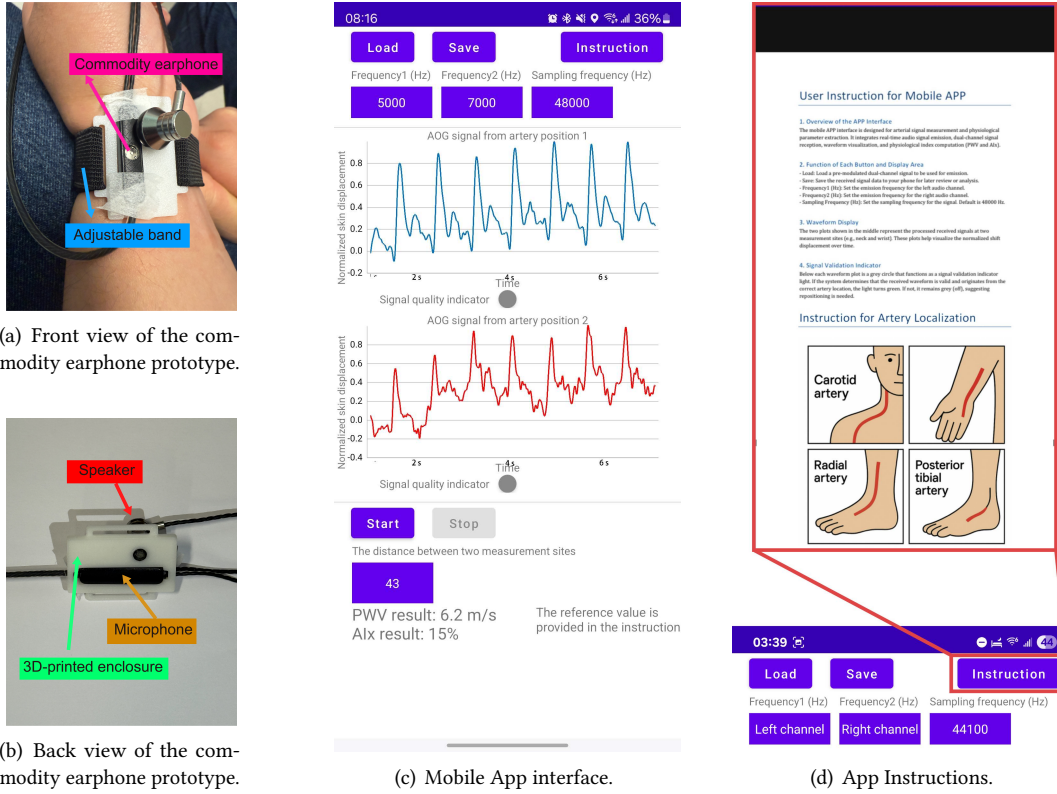


Fig. 7. The hardware and software prototypes of our system. (a) Front view of the commercial earphone with 3D-printed enclosure and adjustable band; (b) Rear view with integrated speaker and microphone; (c) Mobile app showing real-time waveforms, controls, and PWV/AIx results; (d) Built-in user instructions in the app.

includes two speakers and one microphone. The splitter is then plugged into a smartphone directly or via a USB-C adapter. While this setup enables two microphones to operate simultaneously, the signals are still merged into a single input channel on the smartphone due to audio hardware constraints [12, 17, 51, 57].

To separate these signals, we introduce a software solution based on Orthogonal Frequency Division Multiplexing (OFDM). As illustrated in Fig. 5(b), we design the transmitted acoustic signals as two distinct single-tone waveforms: one at frequency f_1 modulated onto the left audio channel, and another at frequency f_2 modulated onto the right channel of the splitter. A sufficient frequency gap between f_1 and f_2 is maintained to avoid aliasing and ensure signal separability. These two signals are simultaneously transmitted through two pairs of earphones placed at different arterial sites. The reflections from surrounding skins at both sites are captured by the respective microphones and mixed into a single input channel on the smartphone. To separate the individual signals corresponding to each transmission frequency, we apply band-pass FIR filters with a cutoff range of $[f_1 - 5 \text{ Hz}, f_1 + 5 \text{ Hz}]$ and $[f_2 - 5 \text{ Hz}, f_2 + 5 \text{ Hz}]$, respectively. The separated signals are then independently processed to estimate AOG signals from each arterial site. Fig. 6 shows the normalized skin velocity and displacement captured at the wrist and neck after applying our signal separation process. These results demonstrate the ability of our system to simultaneously and independently monitor tissue oscillations at multiple arterial locations, enabling accurate two-point sensing for PWV computation.

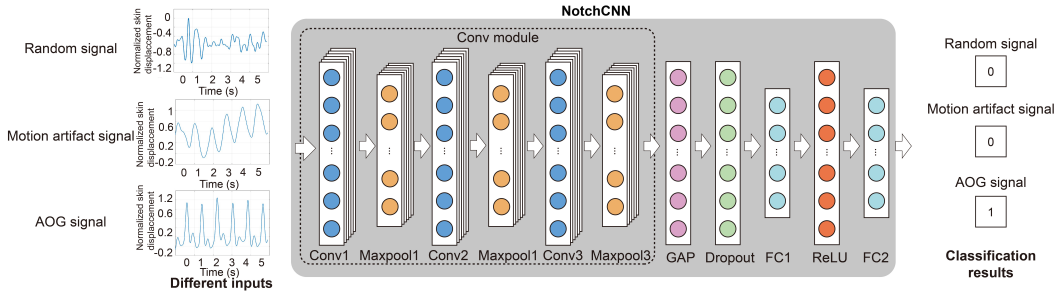


Fig. 8. The architecture of our signal quality assessment model NotchCNN. Three input examples are provided, including random, motion artifact, or AOG signal. The output determines whether the input is a clear and reliable AOG signal.

5.4 Mobile Application and Signal Matching

Accurate artery localization is essential for reliable signal acquisition, but it remains a major challenge, especially for untrained users. While arteries are near the skin surface, their pulsation-induced displacements are extremely subtle and often obscured by tissue damping, particularly in individuals with higher body fat.

To address this, we developed a mobile application that provides real-time interactive feedback to guide users during arterial health measurements. To enhance usability and ensure consistent placement, we designed a 3D-printed enclosure that integrates both the speaker and microphone from a standard earphone and attaches to an adjustable band, as illustrated in Fig. 7(a) and Fig. 7(b).

5.4.1 Mobile Application. As shown in Fig. 7(c), we developed a mobile app to help with arterial localization and display measurement results. It guides users through sensor placement and parameter setup, with both text- and video-based instructions available in the built-in Instruction module (Fig. 7(d)). Upon pressing the “Start” button, the system begins emitting acoustic signals through the speakers and simultaneously records reflections via the microphones. The acquired data is processed directly on the smartphone, with real-time displacement waveforms from both sites visualized in the interface. To assess signal quality, we implement a simple convolutional neural network that evaluates the characteristic patterns of the AOG signals and determines whether they are suitable for computing PWV and AIx. If the signal is valid, a green indicator confirms correct positioning. If no clear arterial signals are detected due to misalignment or motion artifacts, the indicator remains gray, prompting the user to adjust the device and retry until the correct artery site is found.

5.4.2 Signal Quality Assessment. As illustrated in Fig. 8, misalignment with the arterial site leads to the collection of random or noisy signals instead of valid AOG waveforms. Additionally, motion artifacts such as muscle vibrations during measurement can further distort the signal and reduce its reliability.

To ensure signal quality, we leverage a key characteristic of AOG signals—the presence of a pronounced dicrotic notch [20], which reflects the backward wave component and serves as a distinctive feature (see Fig. 4(c)). Inspired by the approach in [24], we design a lightweight one-dimensional convolutional neural network (1D-CNN), called NotchCNN, optimized for time-series signal classification on mobile devices. NotchCNN performs real-time validation by detecting whether a clear and consistent AOG pattern is present, enabling robust signal quality assessment during measurement.

The complete architecture of NotchCNN is shown in Fig. 8. It consists of three sequential 1D convolutional layers, each followed by batch normalization, ReLU activation, and max pooling. The first layer (Conv1) takes a single-channel input and applies 32 filters with a kernel size of 7 to detect basic waveform features, such as rising/falling edges and the shape of the systolic peak. The second layer (Conv2) builds on these features using 64 filters of size 5 to learn compound structures involving both the systolic peak and the dicrotic notch. The

Table 2. List of the off-the-shelf smartphones and 3.5mm earphones.

	Smartphone		Earphone
1	Samsung S9	1	Sony MDR-EX15AP
2	Motorola Edge 2020	2	Sephia SP3060
3	Pixel 4	3	Apple Earpods
4	Pixel 8	4	JBL TUNE 110
5	Samsung S22	5	Sennheiser CX80S
6	Sony Xperia 10	6	Amazon Basics

third layer (Conv3) uses 128 filters with a kernel size of 3 to extract higher-level features related to waveform periodicity and overall morphology. Each convolutional stage includes batch normalization to stabilize training and max pooling (kernel size 2) to reduce temporal resolution.

After the convolutional layers, a global average pooling layer (GAP) compresses the temporal dimension into a 128-dimensional feature vector. A dropout layer (rate 0.3) helps prevent overfitting, and ReLU is used as the activation function throughout. Finally, two fully connected layers reduce the feature vector from 128 to 64, then to 2 output logits for binary classification. This architecture efficiently captures both local and global characteristics of the AOG signal, making it well-suited for real-time signal quality assessment on mobile devices.

In addition, we adopt the cross-entropy loss function [35] for binary classification. The final layer of the network outputs a two-dimensional logit vector $\mathbf{z} = [z_0, z_1]$ for each input signal. The probability of class $c \in \{0, 1\}$ is computed using the softmax function:

$$p_c = \frac{\exp(z_c)}{\exp(z_0) + \exp(z_1)}, \quad (9)$$

where p_c is the predicted probability for class c , and the ground truth label is represented by an integer $y \in \{0, 1\}$. Since this is a binary classification task, the predicted probabilities satisfy $p_0 + p_1 = 1$. Using a one-hot encoding scheme, we define $y_c = 1$ if c is the correct class, and $y_c = 0$ otherwise. The cross-entropy loss is then defined as:

$$\mathcal{L} = - \sum_{c=0}^1 y_c \log(p_c). \quad (10)$$

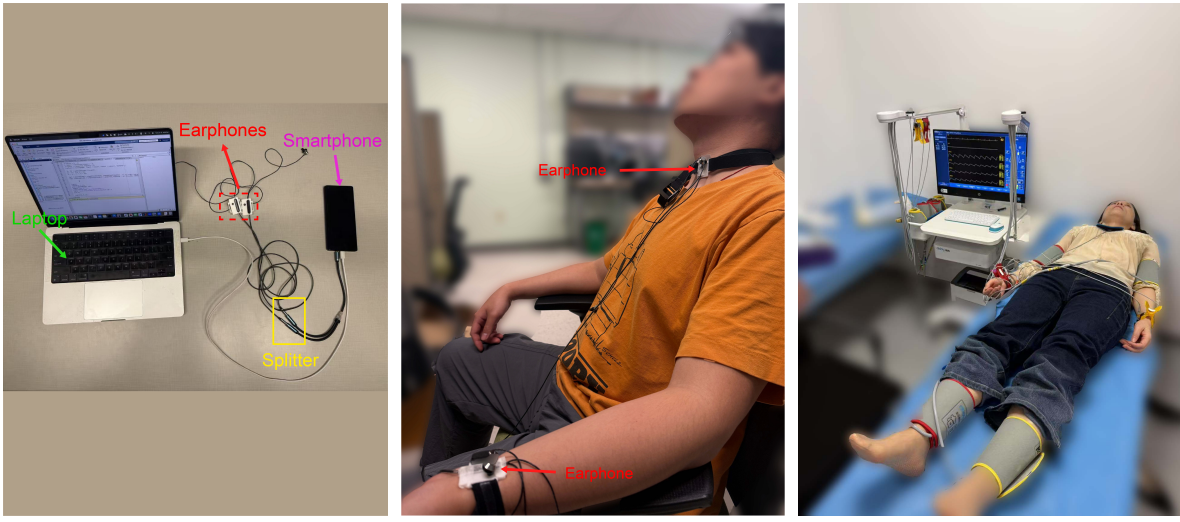
5.5 Clinical Metric Estimation

After acquiring AOG signals from two measurement sites, our system computes PWV using the method described in Sec. 3.1. Specifically, it identifies the systolic peaks within the same cardiac cycle at each site and calculates the interval as the time difference between these peaks, as illustrated in Fig. 6(b). To enhance robustness and reduce variability, the system averages PWV values over five consecutive cardiac cycles.

For AIx estimation, the system follows the approach outlined in Sec. 3.2, using the AOG signal collected from the radial artery. Likewise, our system computes AIx across five consecutive cardiac cycles and reports the average value to improve measurement reliability.

6 IMPLEMENTATION

We implement a proof-of-concept system using commodity smartphone and earphones equipped with a built-in microphone. We further test various combinations of different smartphone and earphone brands, as shown in Table 2. Signal processing and analysis are performed using MATLAB on a MacBook Pro equipped with an M2 CPU and 32GB of memory. We also develop an Android app as shown in Fig. 7(c) to process the data in real time.



(a) The illustration of our device and setup. (b) The measurement from our device. (c) The measurement from the medical device.

Fig. 9. The illustration of the experiment setup.

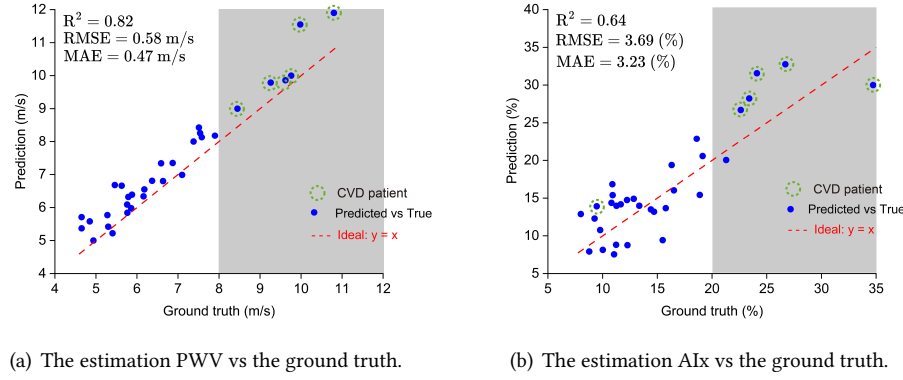
In our experiments, unless otherwise specified, the default configuration consists of a Motorola Edge 2020 smartphone and two Sennheiser CX80S earphones. The OFDM signal used combines 5 kHz and 7 kHz frequencies. A headphone splitter is employed to connect the same pair of earphones to the smartphone, enabling simultaneous data collection from two measurement sites, as shown in Fig. 9(a) and Fig. 9(b).

Ground-truth. We use the dedicated medical device Chioy VBP-9 to obtain the ground truth, as shown in Fig. 9(c). Chioy VBP-9 is widely recognized for its clinical accuracy, exhibiting a correlation of over 98% with invasive catheter-based measurements. It determines PWV by deploying tension sensors at two anatomical locations—the arm (brachial artery) and the ankle—and simultaneously capturing pulse wave signals. However, due to differences in vascular elasticity and blood pressure transmission pathways across these segments, direct comparisons with other arterial paths are not straightforward. Based on clinical guidelines from YAMASHINA et al. [63], the measured brachial-ankle PWV is typically multiplied by a factor of 0.56 to approximate the PWV value between the carotid and radial arteries (neck to wrist). AIx is also derived from the same pulse waveform.

7 EVALUATION

We first conduct a field study in clinic settings to evaluate the overall system performance (Sec. 7.1). We then run a batch of micro-benchmarks to understand the impact of various factors (e.g., ambient noise, subject diversity) on system performance (Sec. 7.2). Finally, we conducted a user study to evaluate the usability of our system among untrained and non-medical users (Sec. 7.3).

Evaluation Metrics. We employ both Root Mean Square Error (RMSE) and the coefficient of determination (R^2 score) to evaluate the performance of our AOG-based system against the ground truth. To maintain consistency across all experiments, unless otherwise specified, we use 5 kHz and 7 kHz OFDM signals with a voltage gain of 80 as the default acoustic configuration. Specifically, the 5 kHz signal is assigned to the left audio channel and attached to the wrist, while the 7 kHz signal is assigned to the right channel and attached to the neck. The sampling frequency is set to 48 kHz, and each session involves continuous data collection lasting 30 seconds. To ensure reliability, every experiment is repeated five times.



(a) The estimation PWV vs the ground truth.

(b) The estimation AIx vs the ground truth.

Fig. 10. An illustration of PWV and AIx measurements against the ground-truth. The PWV higher than 8 m/s (highlighted in gray) or the AIx higher than 20% indicates the higher likelihood of cardiovascular diseases [5, 29].

7.1 Overall System Performance

We recruit 32 individuals from the hospital for system evaluation. The cohort consisted of 10 individuals aged 20-29, 7 aged 30-39, 5 aged 40-49, 5 aged 50-59, and 5 aged 60-70. Among them, 17 were male, and the remaining 15 were female. A retrospective review of their clinical records reveals that 6 participants have cardiovascular disease-related conditions, providing a diverse sample for validating the system under both healthy and pathological scenarios. While the experiments are primarily conducted in a hospital setting to allow comparison with dedicated medical devices, we believe the results are also applicable in home environments. The average ambient noise level during the experiments is around 50 dB. All experimental procedures are approved by the Institutional Review Board (IRB) at University of Massachusetts Amherst.

7.1.1 PWV and AIx Estimation Accuracy. Fig. 10(a) illustrates the comparison between the estimated PWV and the ground truth values. Each data point corresponds to a measurement from an individual, totaling 32 measurements, with measurements from six individuals diagnosed with cardiovascular diseases indicated by green circles. From this figure, we observe that our method achieves a mean absolute error (MAE) of less than 0.5 m/s across 32 individuals. These results remain well within the clinically acceptable error margin for PWV measurements (< 1 m/s) [10, 34]. We further examine system performance separately for 26 healthy individuals and six individuals with cardiovascular diseases. Our system achieved an RMSE of 0.55 m/s among healthy individuals, with a slight increase to 0.72 m/s for individuals with cardiovascular diseases. Nevertheless, all values measured within these two groups are within the clinically acceptable range. These results demonstrate the high accuracy of our system.

Fig. 10(b) presents the results for AIx estimation. From this figure, we observe that our method achieves a MAE of less than 3.3%, satisfying established medical standards and remaining well within the clinically acceptable error range for AIx estimation (less than 6%) [10, 34]. The corresponding RMSE and R^2 values further demonstrate the accuracy and reliability of our AIx predictions. We also examine system performance separately for 26 healthy individuals and six individuals with cardiovascular diseases. Our system achieves an RMSE of 3.18% among healthy individuals, with a slight increase to 5.07% for individuals with cardiovascular diseases.

The observed increase in RMSE for both PWV and AIx between healthy individuals and those with cardiovascular diseases can be attributed to underlying physiological changes. Abnormally high PWV and AIx are generally indicative of conditions such as arteriosclerosis. Cardiovascular diseases often lead to arteriosclerosis, which not only elevates the result but also reduces arterial dilation in response to the heartbeat. This diminished

[‡]The IRB number is 6006.

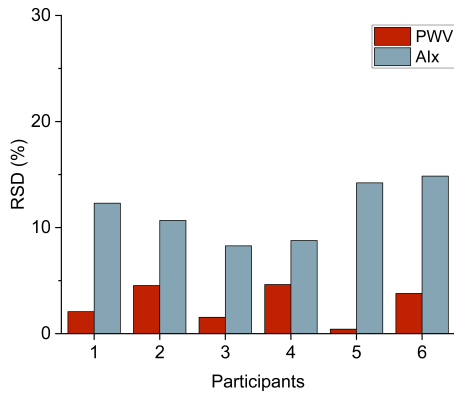


Fig. 11. The result of repeatability.

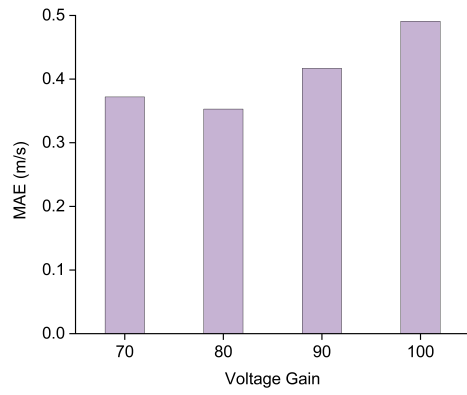


Fig. 12. Impact of the different volume.

arterial elasticity, in turn, affects the heartbeat waveform captured by our system at a single measurement site. Moreover, the growth in RMSE is particularly evident among elderly individuals. This can be further attributed to increased skin laxity with age, which compromises the stability of device-skin contact and alignment with the artery, ultimately leading to higher measurement errors.

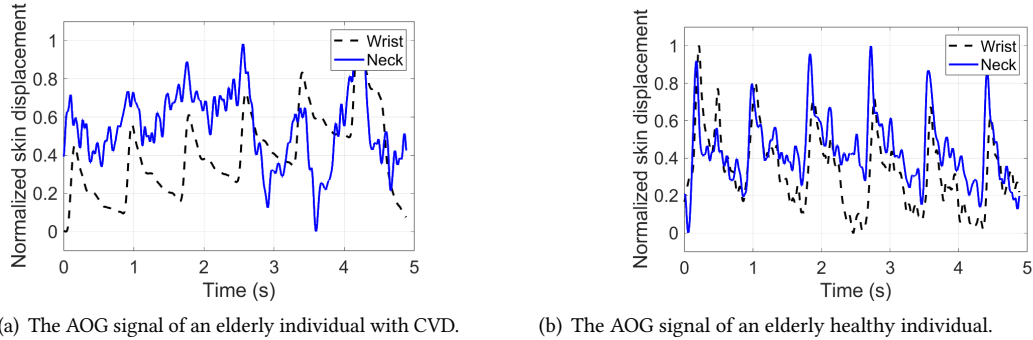
7.1.2 Measurement Stability. Measurement stability is a key performance metric for any physiological monitoring system. To assess the stability of our system, we recruited six volunteers, each of whom performed five PWV measurements, with 10-minute intervals between tests. Throughout the testing period, participants were instructed to remain relatively at rest so that their PWVs are stable. Hence a stable device should report consistent PWV readings across five measurement sessions for each participant. We evaluate the measurement stability using Relative Standard Deviation (RSD). Fig. 11 presents the RSD results for each volunteer. The findings demonstrate the high stability of our system, with individual RSD values ranging from as low as 0.42% to as high as 4.54%. The RSD values for AIx, on the other hand, are higher, ranging from 8.28% to 14.86%. These RSD values for AIx also meet the allowable limit of 20% for bio-analytical method validation [3].

One may wonder why there is a performance gap between the RSD of PWV and that of AIx. PWV is determined by measuring the appearance time of the systolic peak which is relatively stable and easy to detect. Hence its RSD is relatively small. In contrast, AIx is calculated as the amplitude ratio of the dicrotic notch to the systolic peak. During the measurement process, external factors such as human movement can distort the waveform, and the dicrotic notch, which is inherently weaker, is particularly vulnerable to these disturbances. As a result, the values used for AIx calculation are more easily susceptible to body motions, leading to more significant variations.

7.2 Micro-benchmarks

We conducted a batch of micro-benchmarks to assess the impact of various factors on our system performance.

7.2.1 Impact of signal volume. We first assess the impact of signal volume on PWV measurement accuracy. We control the signal volume by varying the voltage gain from 70 to 105. Values outside this range fail to produce detectable AOG signals—either due to exceeding the hardware’s effective operating limit at high gain or due to insufficient excitation at low gain. The testing results are presented in Fig. 12. We observed that our system achieves the highest PWV measurement accuracy when the voltage gain is set to 80. As the voltage gain grows, the speaker tends to produce self-excited vibrations, introducing strong noise that degrades measurement accuracy. On the other hand, when the voltage gain is too low, the already weak reflection signal becomes more susceptible



(a) The AOG signal of an elderly individual with CVD. (b) The AOG signal of an elderly healthy individual.

Fig. 13. AOG Waveforms of Elderly Individuals: CVD vs. Healthy.

to environmental and system noise, also reducing accuracy. We adopt 80 voltage gain as our default setting for all the other experiments.

7.2.2 Impact of subject diversity. Next, we assess the system performance across subject groups categorized by BMI, gender, age, skin tone, and height, based on 32 individuals from the hospital. Fig. 13 shows the AOG waveform results for three different subjects.

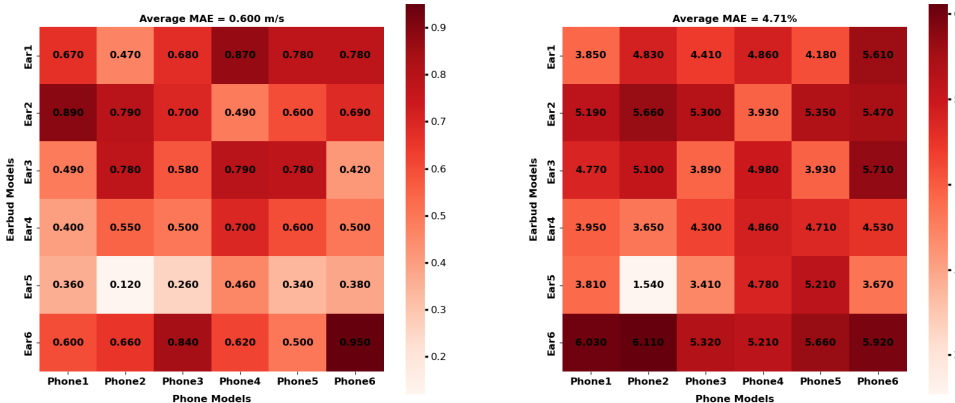
We have three observations from the result shown in Table 3:

- First, AOG consistently provides accurate estimations of PWV and AIx across diverse demographic groups. The average MAE for PWV remains below 0.8 m/s, while the average MAE for AIx is under 7%.
- Second, BMI has a significant impact on system performance. Specifically, for PWV estimation, when BMI is less than 25, the MAE is 0.33 m/s. As BMI increases, the MAE for PWV also rises. Notably, when BMI reaches 30, the MAE increases to 0.73 m/s. A similar trend is observed for AIx estimation. This is because a higher BMI typically corresponds to greater adipose tissue, which dampens arterial pulsations and weakens tissue oscillations, thereby reducing measurement accuracy.
- Third, we observe a slight decline in accuracy among older individuals. For example, when participants are younger than 30 years old, the MAE for PWV is 0.37 m/s. For participants aged 30–60 years, the MAE increases to 0.48 m/s, and for those older than 60 years, it further rises to 0.87 m/s. Representative AOG waveforms are shown in Fig. 13(b) for a healthy elderly individual and in Fig. 13(a) for an elderly individual with CVD. Notably, the MAE exceeds 0.5 m/s for participants older than 30 years. A similar trend is observed for AIx estimation. This decline in accuracy may be attributed to increased skin laxity with age, which affects the stability of device-skin contact and alignment with the artery, leading to higher measurement errors. Furthermore, by comparing Fig. 13(b) and Fig. 13(a), we observe that the dicrotic notch in the waveform of the CVD individual is not clearly visible. This is because, in elderly individuals with CVD, the arterial walls become thicker and stiffer, leading to reduced vascular compliance and elevated PWV. As a result, backward waves return earlier—often before the heart has completed contraction or just prior to valve closure—overlapping with the forward wave. Consequently, the dicrotic notch becomes less distinct or appears blunted in the AOG waveform [46].
- Fourth, height and skin tone do not appear to noticeably affect measurement accuracy. The MAE for PWV remains below 0.5 m/s, and the MAE for AIx remains below 4.5% across different heights and skin tones, indicating that variations in these factors do not significantly influence the measurement results.

Finally, to evaluate the impact of posture, we invite four participants in our clinical studies and measure the MAE of their PWV and AIx under three different postural conditions: standing, sitting, and lying. We found that standing introduces greater error, with the MAE for PWV reaching 0.62 m/s. This is due to gravitational effects that alter blood flow dynamics, leading to increased peripheral vascular resistance and decreased central aortic

Table 3. The comparison of subject diversity.

MAE	Factor																
	BMI			Gender		Age			Skin tone			Height			Posture		
	25	25-30	30	Male	Female	30 yrs	30-60 yrs	60 yrs	Lighter	Common	Darker	165 cm	165-180 cm	180 cm	Standing	Sitting	Lying
PWV (m/s)	0.33	0.49	0.73	0.42	0.46	0.37	0.48	0.87	0.44	0.47	0.41	0.44	0.42	0.44	0.62	0.40	0.39
AIx (%)	3.79	4.24	5.84	4.28	4.11	4.08	4.49	7.58	3.87	4.02	3.99	4.13	4.37	4.12	4.39	3.99	3.92



(a) The MAE of PWV. (b) The MAE of AIx.

Fig. 14. The illustration of different equipment combination.

pressure [48]. In contrast, the errors observed in sitting and lying positions are comparable, with only a 0.01 m/s difference. A similar trend is observed for AIx estimation. This is because the distance from the carotid artery to the radial artery is relatively short compared to other measurement paths, such as from the ankle-brachial artery to the radial artery. Therefore, when sitting, the influence of gravitational acceleration is not significant. Based on these experiment results, we recommend measuring the PWV and AIx either while seated or lying down.

7.2.3 Impact of different combinations. To evaluate the impact of different equipment combinations, we tested various pairings of smartphones and earphones, as shown in Table 2. The results are presented in Fig. 14. We observed that the error across all device combinations exhibited only minor variations. Specifically, the MAE for PWV was consistently less than 1 m/s, with an average MAE of 0.6 m/s. For AIx estimation, the MAE remained below 6%, with an average MAE of less than 4.71%, which meets the medical standards [10, 34]. Notably, when using the same model of earphones with different smartphones, the results remained consistently similar. The minor differences observed are primarily attributed to variations in the analog-to-digital converters (ADCs) and digital-to-analog converters (DACs) across different smartphone models. However, variations appear when comparing different earphone models paired with the same smartphone. The performance varies slightly: the Sennheiser CX80S achieves the highest accuracy, with a difference from the ground truth of less than 0.4 m/s for the MAE of PWV and less than 5.5% for the MAE of AIx. In contrast, the Amazon Basics model exhibits the lowest performance, with the MAE of PWV remaining under 1 m/s and the MAE of AIx under 6%. This discrepancy can be attributed to differences in the frequency response curves of the earphones. Specifically, the Sennheiser CX80S exhibits highly stable phase characteristics, which contribute significantly to its performance.

7.2.4 Impact of ambient noise. We conduct experiments to evaluate the impact of ambient noise on system performance. Specifically, we introduce three types of noise generated by different sources: human conversation (58.1 dB), an air conditioner (70 dB), and a canteen environment (105 dB). Additionally, we play a chirp signal ranging from 5 kHz to 7 kHz near the device as another form of noise. We observe that the PWV and AIx

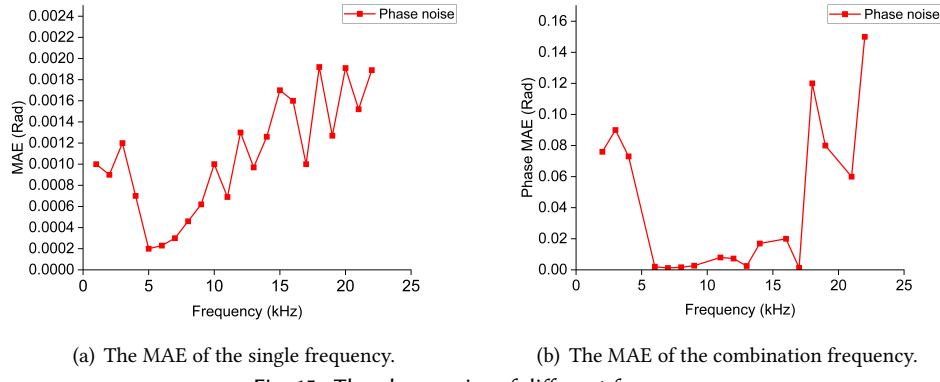


Fig. 15. The phase noise of different frequency.

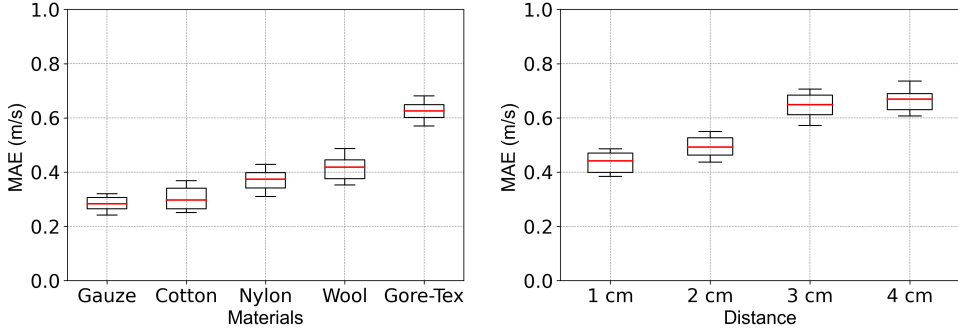


Fig. 16. Performance comparison of PWV estimation across different materials and measurement distances.

measurement errors under these noisy conditions are comparable to those measured in a quiet environment (41.8 dB). This robustness is primarily because ambient noise frequencies are typically above 200 Hz, exceeding the frequency range of physiological signals. Furthermore, our denoising module is specifically designed to effectively eliminate high-frequency noise, thereby minimizing its impact on the measurements. In addition, placing the device directly on the skin creates a relatively enclosed space, isolating measurement results and further reduces susceptibility to external environmental influences.

7.2.5 Impact of hardware. The oscillation resolution of our device is impacted by the phase noise of the speaker. To characterize this impact, we measure the phase noise of our device across the full frequency range from 1 kHz to 22 kHz with a step size of 1 kHz. As shown in Fig. 15(a), we observe that the maximum phase noise occurs at 20 kHz, reaching approximately 0.001 Rad. This equals to $\frac{1}{10}$ of a full oscillation cycle, which is sufficient to resolve the oscillatory motion. This confirms that our system can operate effectively across the full frequency range.

Based on this evaluation, we select 5 kHz, the frequency with the lowest measured phase noise, as one of our channels. To identify the optimal second channel frequency for two-tone operation, we test combinations of 5 kHz with other frequencies ranging from 1 kHz to 22 kHz. To avoid frequency aliasing and harmonic interference, we exclude multiples of 5 kHz (i.e., 1 kHz, 5 kHz, 10 kHz, 15 kHz, and 20 kHz). The results of these frequency combinations are shown in Fig. 15(b). We observe that due to manufacturing differences, the optimal phase noise performance for the combination of 5 kHz and another frequency occurs when the second frequency lies between 4 kHz and 13 kHz. Among these, 7 kHz yields the lowest phase noise, reaching a minimum of 0.0012.

Table 4. Comparison of results from our method at different measurement sites.

	Estimation (m/s)	Ground truth (m/s)	Error (m/s)
Neck-Wrist	5.67	5.97	0.30
Wrist-Ankle	9.93	10.66	0.73

Table 5. The results of long-term measurement.

No.of week \ Value	1	2	3	4	5	6	7	8	9	10	11	12	13	14	15	16
PWV (m/s)	6.35	6.16	6.36	6.13	6.33	6.32	6.15	6.38	6.19	6.13	6.34	6.21	6.42	6.07	6.45	6.06
AIx (%)	13.65	11.66	13.59	11.62	13.54	13.77	11.55	11.73	13.56	11.64	13.63	11.59	14.37	10.92	14.46	10.87

7.2.6 Impact of distance. In real-world scenarios, such as when patients with skin conditions perform self-checks or when doctors examine individuals with skin ulcers or injuries, it is often impractical to attach the device directly to the skin. We explore whether our system can support through-clothing or contactless measurement while maintaining reliable accuracy. To do so, we conduct two experiments: one to assess the impact of different fabric textures, and the other to examine the effect of varying distances between the device and the skin. In both experiments, PWV values are used as the primary evaluation metric to quantify system performance.

Fig. 16(a) shows the results of our MAE for PWV measurements across various fabric textures, including cotton, wool, gauze, nylon, and Gore-Tex. We find that gauze and cotton demonstrate higher accuracy, with MAE values for PWV ranging from 0.24 to 0.32 m/s, as acoustic signals can easily penetrate these materials. In contrast, Gore-Tex exhibits lower accuracy, with MAE values for PWV ranging from 0.57 to 0.69 m/s, likely because it reflects a portion of the acoustic signal. Fig. 16(b) shows the MAE of PWV measurements when measuring at varying distances between the device and the skin, specifically at 1 cm, 2 cm, 3 cm, and 4 cm. As shown in Fig. 16(b), even at a distance of 4 cm, the error is below 0.8 m/s, which satisfies the measurement requirements.

7.2.7 Impact of different measurement sites. We deploy the device on various arterial sites beyond the neck and wrist. These included the dorsal artery of the foot, the femoral artery, and the temporal artery near the ear. Measurements at these additional sites also yield valid PWV values. However, these values differ due to variations in measurement distances and the involvement of different types of arteries—each with distinct elastic properties [46]. Therefore, to validate our system’s performance, we measured the PWV between the neck (carotid artery) and wrist (radial artery), as well as between the wrist (radial artery) and ankle (posterior tibial artery), and compared the results against ground truth measurements for the same individuals. The results are presented in Table 4. Regardless of the measurement location, the estimation errors remained below 7%.

7.2.8 Impact of Long-term measurement. To assess the stability of long-term measurements, we tracked a single user over four months, collecting PWV and AIx data every Sunday night using our system. Results are shown in Table 5. During this period, PWV error fluctuated by less than 0.2 m/s, and AIx error by less than 1.8%, demonstrating the robustness and consistency of the proposed system.

7.3 User Study

To evaluate the usability and user experience of our system for untrained users, we conducted a post-task questionnaire including both Likert-scale items and open-ended questions. As noted by Nielsen and Landauer [47], testing with 5–8 participants is sufficient to uncover approximately 85% of usability issues in a prototype. Following this guideline, our study involved six participants (4 male, 2 female, aged 20–60) with diverse backgrounds, none of whom had any prior medical experience. As shown in Fig. 17, participants rated the system’s usability, comfort, ease of first use, and overall satisfaction. The results indicate that untrained users were able to operate the system effectively with minimal guidance, highlighting its practicality and user-friendliness for daily use. Specifically,

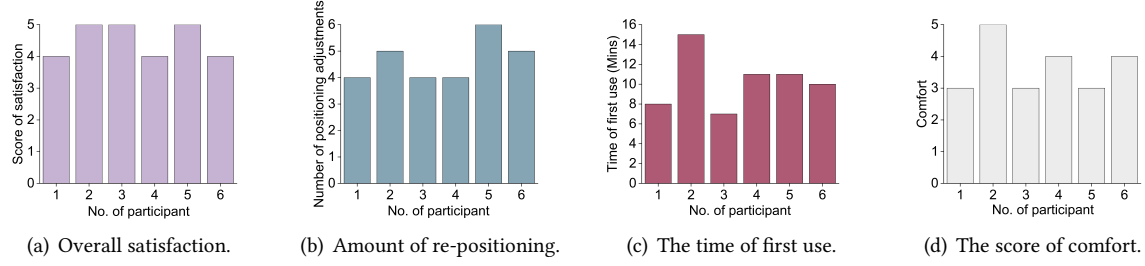


Fig. 17. User study results. (a) Overall satisfaction scores (0 = not satisfied at all, 5 = extremely satisfied). (b) Number of positioning adjustments needed. (c) Time taken to obtain the AOG signal on first use. (d) Comfort ratings reported by participants (0 = very uncomfortable, 5 = extremely comfortable).

the overall satisfaction score was 4.5 out of 5, the average number of positioning adjustments was 4.7, the average time to first successful use was 10.3 minutes, and the average comfort rating is 3.67. Additionally, two participants suggested that the device could be made smaller since the 3D-printed enclosure was somewhat bulky and made it difficult to adjust the position easily.

8 DISCUSSION

System Setup. To use our system, users need a tape measure to determine the distance required for PWV calculation. This distance is measured along the body surface by subtracting the neck-to-heart distance from the heart-to-wrist distance, following standard clinical practices for PWV estimation. In addition, users need to fabricate a 3D-printed enclosure and obtain a wristband. The enclosure is low-cost (under \$0.10), easy to fabricate, and openly available online as an open-source design. The adjustable wristband, used to secure the device, can be purchased on Amazon for about \$1 [4]. The enclosure and band ensure that the earphone's speaker and microphone are properly aligned over the same arterial site. This setup enables untrained users to operate the system independently. Additionally, we found that as long as proper alignment is maintained, simple alternatives such as adhesive tape can be equally effective.

Custom Devices. Our evaluation revealed two limitations that can be addressed in future iterations. First, the nozzle design of commodity earphones prevents the speaker from making direct contact with the skin, which lowers the signal-to-noise ratio (SNR). Second, their large form factor hinders precise positioning at the measurement site, thus reducing accuracy. To address these issues, we developed a low-cost (under \$2) custom sensor featuring an integrated printed circuit board (PCB) that combines both the microphone and speaker, allowing for better skin contact and enhanced SNR. Compared to commodity earphones, the custom device reduces the MAE in PWV estimation from 0.47 m/s to 0.40 m/s and in AIx estimation from 3.23% to 3.02%. Detailed information about the hardware design and corresponding experimental results is provided in the Appendix.

Performance Improvement Strategies. Our experiments indicate that performance degrades for individuals with higher BMI or older age. This is primarily due to physiological factors such as skin laxity and increased subcutaneous fat, which dampen signal quality. To address this, maintaining firm contact between the earphone and the skin is critical for accurate measurements. Additionally, taking multiple measurements and averaging the results can improve reliability in daily use.

Potential Application. Prior studies have shown that systolic blood pressure scales with the square of pulse wave velocity [11, 41]. Additionally, diastolic blood pressure can be estimated using a combined model that incorporates both pulse wave velocity and the augmentation index [30]. These findings indicate that our system has the potential to support blood pressure estimation. In future work, we plan to collect data from a diverse population to further develop and validate this application.

9 CONCLUSION

In this paper, we explore the feasibility of using acoustic sensing with low-cost wired earphones to monitor arterial health by measuring Pulse Wave Velocity (PWV) and Augmentation Index (AIx). To achieve this, we leverage Doppler shift to capture subtle skin displacements induced by arterial pulsation and construct the corresponding Acoustoscillogram (AOG) waveform. To address the challenge of capturing AOG signals from two measurement sites within the same cardiac cycle, we propose a hardware-software co-design. This involves using two pairs of wired earphones with line-in microphones placed at different arterial sites, along with an Orthogonal Frequency-Division Multiplexing (OFDM) strategy to separate the reflected signals for dual-site AOG extraction. To enhance usability for individuals, we also developed a mobile application designed specifically to support untrained users. We validate our system using clinical data from 32 participants, comparing the results against measurements from a medical-grade reference device. Experimental results demonstrate that our system achieves a PWV error of less than 0.5 m/s and an AIx error of less than 4%, satisfying established medical standards.

10 Acknowledgments

We gratefully acknowledge the anonymous reviewers for their constructive comments and suggestions. We would also like to thank Ruoxue Wu, Yue Pei and Dr. Hongyu Liu for their valuable support during the course of this research. This work was supported in part by the National Science Foundation (NSF, Grant No. 2337537) and the National Institutes of Health (Grant No. R01HD114147), and the National Institute on Aging of the NIH (Grant No. P30AG073107).

References

- [1] Fadel Adib and Dina Katabi. 2013. See through walls with WiFi!. In *Proceedings of the ACM SIGCOMM 2013 conference on SIGCOMM* (Hong Kong, China) (SIGCOMM '13). Association for Computing Machinery, New York, NY, USA, 75–86.
- [2] Fadel Adib, Hongzi Mao, Zachary Kabelac, Dina Katabi, and Robert C. Miller. 2015. Smart Homes that Monitor Breathing and Heart Rate. In *Proceedings of the 33rd Annual ACM Conference on Human Factors in Computing Systems (CHI '15)*. ACM. doi:10.1145/2702123.2702200
- [3] European Medicines Agency. 2009. Bioanalytical method validation - Scientific guideline. online.
- [4] Amazon. 2025. Adjustable Straps For Wigs And Making Wigs, Adjustable Wig Bands (6pcs). Online. https://www.amazon.com/Adjustable-Elastic-WigsijjEAdjustable-BandsijjEWig-StrapsijjL1/dp/B09X5CTPTH/ref=sr_1_2?dib=eyJ2IjoiMSJ9_wqp9yUCxjL_u4EcB8XMGNyB3WEkldgii7a7wrKYnbcqUsgEu5hXOIC2SAw0Ztrt3zNfotgIeugoMxzBRL48rV0S13O9XsDYultGpVmQEM.SAar9DNoT2e0rtrl3yUCCTZXQ_JuO3cXOLit3zWRTm4&dib_tag=se&qid=1753841921&refinements=p_89:JIUSERLU&sr=8-2&srs=69653768011&th=1
- [5] Daniel Baier, Andrej Teren, Kerstin Wirkner, Markus Loeffler, and Markus Scholz. 2018. Parameters of pulse wave velocity: determinants and reference values assessed in the population-based study LIFE-Adult. *Clinical research in cardiology : official journal of the German Cardiac Society* 107 (Nov. 2018), 1050–1061. Issue 11. doi:10.1007/s00392-018-1278-3
- [6] Ananta Narayanan Balaji, Andrea Ferlini, Fahim Kawsar, and Alessandro Montanari. 2023. Stereo-BP: Non-Invasive Blood Pressure Sensing with Earables. In *Proceedings of the 24th International Workshop on Mobile Computing Systems and Applications* (Newport Beach, California) (HotMobile '23). Association for Computing Machinery, New York, NY, USA, 96–102. doi:10.1145/3572864.3580341
- [7] Daniel Bia and Yanina Zócalo. 2021. Physiological Age- and Sex-Related Profiles for Local (Aortic) and Regional (Carotid-Femoral, Carotid-Radial) Pulse Wave Velocity and Center-to-Periphery Stiffness Gradient, with and without Blood Pressure Adjustments: Reference Intervals and Agreement between Methods in Healthy Subjects (3–84 Years). *Journal of Cardiovascular Development and Disease* 8, 1 (Jan. 2021), 3. doi:10.3390/jcdd8010003
- [8] Pierre Boutouyrie, Assya Achouba, Patrick Trunet, and Stephane Laurent. 2010. Amlodipine-Valsartan Combination Decreases Central Systolic Blood Pressure More Effectively Than the Amlodipine-Atenolol Combination: The EXPLOR Study. *Hypertension* 55, 6 (June 2010), 1314–1322. doi:10.1161/hypertensionaha.109.14899
- [9] Nam Bui, Nhat Pham, Jessica Jacqueline Barnitz, Zhanan Zou, Phuc Nguyen, Hoang Truong, Taeho Kim, Nicholas Farrow, Anh Nguyen, Jianliang Xiao, Robin Deterding, Thang Dinh, and Tam Vu. 2019. eBP: A Wearable System For Frequent and Comfortable Blood Pressure Monitoring From User's Ear. In *The 25th Annual International Conference on Mobile Computing and Networking (Los Cabos, Mexico) (MobiCom '19)*. Association for Computing Machinery, New York, NY, USA, Article 53, 17 pages. doi:10.1145/3300061.3345454
- [10] Mark Butlin and Ahmad Qasem. 2016. Large Artery Stiffness Assessment Using SphygmoCor Technology. *Pulse* 4, 4 (2016), 180–192. doi:10.1159/000452448

- [11] Richard Byfield, Morgan Miller, Jonathan Miles, Giovanna Guidoboni, and Jian Lin. 2022. Towards Robust Blood Pressure Estimation From Pulse Wave Velocity Measured by Photoplethysmography Sensors. *IEEE Sensors Journal* 22 (2022), 2475–2483. Issue 3. doi:[10.1109/JSEN.2021.3134890](https://doi.org/10.1109/JSEN.2021.3134890)
- [12] Shirui Cao, Dong Li, Sunghoon Ivan Lee, and Jie Xiong. 2023. PowerPhone: Unleashing the Acoustic Sensing Capability of Smartphones. In *Proceedings of the 29th Annual International Conference on Mobile Computing and Networking*. 1–16.
- [13] Yetong Cao, Huijie Chen, Fan Li, and Yu Wang. 2021. Crisp-BP: continuous wrist PPG-based blood pressure measurement. In *Proceedings of the 27th Annual International Conference on Mobile Computing and Networking* (New Orleans, Louisiana) (*MobiCom '21*). Association for Computing Machinery, New York, NY, USA, 378–391. doi:[10.1145/3447993.3483241](https://doi.org/10.1145/3447993.3483241)
- [14] Andrew M. Carek, Jordan Conant, Anirudh Joshi, Hyolim Kang, and Omer T. Inan. 2017. SeismoWatch: Wearable Cuffless Blood Pressure Monitoring Using Pulse Transit Time. *Proceedings of the ACM on Interactive, Mobile, Wearable and Ubiquitous Technologies* 1, 3 (Sept. 2017), 1–16. doi:[10.1145/3130905](https://doi.org/10.1145/3130905)
- [15] Tao Chen, Yongjie Yang, Xiaoran Fan, Xiuzhen Guo, Jie Xiong, and Longfei Shangguan. 2024. Exploring the Feasibility of Remote Cardiac Auscultation Using Earphones. In *Proceedings of the 30th Annual International Conference on Mobile Computing and Networking (ACM MobiCom '24)*. ACM, 357–372. doi:[10.1145/3636534.3649366](https://doi.org/10.1145/3636534.3649366)
- [16] Shein-Chung Chow, Jun Shao, Hansheng Wang, and Yuliya Lokhnygina. 2017. *Sample Size Calculations in Clinical Research: Third Edition*. Chapman and Hall/CRC. doi:[10.1201/9781315183084](https://doi.org/10.1201/9781315183084)
- [17] Cirrus Logic Incorporated 2019. CS35L41/Cirrus Logic. Cirrus Logic Incorporated. <https://master-nq.webp2.cirrus.com/products/cs35l41/>
- [18] Zygmunt Domagala, Joanna Grzelak, Natalie Pospiech, Nicole Hunter, Jakub Klekowski, Agnieszka Lach, Katarzyna Stój, Bożena Kuc-Darak, and Miroslaw Trzaska. 2021. Ultrasound evaluation of the radial artery in young adults – A pilot study. *Annals of Anatomy - Anatomischer Anzeiger* 238 (Nov. 2021), 151763. doi:[10.1016/j.ananat.2021.151763](https://doi.org/10.1016/j.ananat.2021.151763)
- [19] DUKABEL. 2025. DUKABEL Headphone Splitter. https://www.amazon.com/Headphone-Splitter-Gold-Plated-2-Female-DuKabel/dp/B07FBBBXW?ref_=ast_sto_dp&th=1
- [20] Xiaoran Fan, David Pearl, Richard Howard, Longfei Shangguan, and Trausti Thormundsson. 2023. APG: Audioplethysmography for Cardiac Monitoring in Hearables. In *Proceedings of the 29th Annual International Conference on Mobile Computing and Networking (ACM MobiCom '23)*. ACM, 1–15. doi:[10.1145/3570361.3613281](https://doi.org/10.1145/3570361.3613281)
- [21] Giancarlo Fortino and Valerio Giampà. 2010. PPG-based methods for non invasive and continuous blood pressure measurement: an overview and development issues in body sensor networks. *2010 IEEE International Workshop on Medical Measurements and Applications*, 10–13. doi:[10.1109/MEMEA.2010.5480201](https://doi.org/10.1109/MEMEA.2010.5480201)
- [22] Cristina Giannattasio, Monica Failla, Alessandra Grappiolo, Marco Bigoni, Stefano Carugo, Matteo Denti, and Giuseppe Mancia. 1998. Effects of Prolonged Immobilization of the Limb on Radial Artery Mechanical Properties. *Hypertension* 32, 3 (Sept. 1998), 584–587. doi:[10.1161/01.hyp.32.3.584](https://doi.org/10.1161/01.hyp.32.3.584)
- [23] Cheng-Yan Guo, Wen-Yao Huang, Hao-Ching Chang, and Tung-Li Hsieh. 2023. Calibrating Oxygen Saturation Measurements for Different Skin Colors Using the Individual Typology Angle. *IEEE Sensors Journal* 23, 15 (Aug. 2023), 16993–17001. doi:[10.1109/jsen.2023.3288151](https://doi.org/10.1109/jsen.2023.3288151)
- [24] Unsoo Ha, Salah Assana, and Fadel Adib. 2020. Contactless seismocardiography via deep learning radars. In *MobiCom '20: The 26th Annual International Conference on Mobile Computing and Networking, London, United Kingdom, September 21–25, 2020*. ACM, 62:1–62:14. doi:[10.1145/3372224.3419982](https://doi.org/10.1145/3372224.3419982)
- [25] Christian Holz and Edward J. Wang. 2017. Glabella: Continuously Sensing Blood Pressure Behavior using an Unobtrusive Wearable Device. *Proceedings of the ACM on Interactive, Mobile, Wearable and Ubiquitous Technologies* 1, 3 (Sept. 2017), 1–23. doi:[10.1145/3132024](https://doi.org/10.1145/3132024)
- [26] Iván G Horváth, Ádám Németh, Zsófia Lenkey, Nicola Alessandri, Fabrizio Tufano, Pál Kis, Balázs Gaszner, and Attila Cziráki. 2010. Invasive validation of a new oscillometric device (Arteriograph) for measuring augmentation index, central blood pressure and aortic pulse wave velocity. *Journal of Hypertension* 28, 10 (Oct. 2010), 2068–2075. doi:[10.1097/hjh.0b013e32833c8a1a](https://doi.org/10.1097/hjh.0b013e32833c8a1a)
- [27] Qingyong Hu, Qian Zhang, Hao Lu, Shun Wu, Yuxuan Zhou, Qianyi Huang, Huangxun Chen, Ying-Cong Chen, and Ni Zhao. 2024. Contactless Arterial Blood Pressure Waveform Monitoring with mmWave Radar. *Proc. ACM Interact. Mob. Wearable Ubiquitous Technol.* (21 11 2024), 1–29. doi:[10.1145/3699781](https://doi.org/10.1145/3699781)
- [28] Xiaonan Hui and Edwin C. Kan. 2017. Monitoring vital signs over multiplexed radio by near-field coherent sensing. *Nature Electronics* 1, 1 (Nov. 2017), 74–78. doi:[10.1038/s41928-017-0001-0](https://doi.org/10.1038/s41928-017-0001-0)
- [29] Julie H. Janner, Nina S. Godtfredsen, Steen Ladelund, Jørgen Vestbo, and Eva Prescott. 2010. Aortic Augmentation Index: Reference Values in a Large Unselected Population by Means of the SphygmoCor Device. *American Journal of Hypertension* 23, 2 (02 2010), 180–185. doi:[10.1038/ajh.2009.234](https://doi.org/10.1038/ajh.2009.234) arXiv:https://academic.oup.com/ajh/article-pdf/23/2/180/11199019/23_2_180.pdf
- [30] Mohamad Kachuee, Mohammad Mahdi Kiani, Hoda Mohammadzade, and Mahdi Shabany. 2015. Cuff-less high-accuracy calibration-free blood pressure estimation using pulse transit time. In *2015 IEEE International Symposium on Circuits and Systems (ISCAS)*. IEEE, 1006–1009. doi:[10.1109/iscas.2015.7168806](https://doi.org/10.1109/iscas.2015.7168806)
- [31] Dhruv S. et al. Kazi. 2024. Forecasting the Economic Burden of Cardiovascular Disease and Stroke in the United States Through 2050: A Presidential Advisory From the American Heart Association. *Circulation* 150, 4 (July 2024). doi:[10.1161/cir.0000000000001258](https://doi.org/10.1161/cir.0000000000001258)

- [32] Matthew D. Keller, Brandon Harrison-Smith, Chetan Patil, and Mohammed Shahriar Arefin. 2022. Skin colour affects the accuracy of medical oxygen sensors. *Nature* 610, 7932 (Oct. 2022), 449–451. doi:10.1038/d41586-022-03161-1
- [33] Lucas Klauth, Andreas Mühlen, Andreas Kitzig, Edwin Naroska, and Gudrun Stockmanns. 2023. Optimization and evaluation of a mobile IMU-based ballistocardiography system. *Current Directions in Biomedical Engineering* 9, 1 (Sept. 2023), 678–681. doi:10.1515/cdbme-2023-1170
- [34] S. Laurent, J. Cockcroft, L. Van Bortel, P. Boutouyrie, C. Giannattasio, D. Hayoz, B. Pannier, C. Vlachopoulos, I. Wilkinson, and H. Struijker-Boudier. 2006. Expert consensus document on arterial stiffness: methodological issues and clinical applications. *European Heart Journal* 27, 21 (Sept. 2006), 2588–2605. doi:10.1093/eurheartj/ehl254
- [35] Yann LeCun, Léon Bottou, Yoshua Bengio, and Patrick Haffner. 1998. Gradient-based learning applied to document recognition. *Proc. IEEE* 86, 11 (1998), 2278–2324. doi:10.1109/5.726791
- [36] Dong Li, Jialin Liu, Sunghoon Ivan Lee, and Jie Xiong. 2020. FM-track: pushing the limits of contactless multi-target tracking using acoustic signals. In *Proceedings of the 18th Conference on Embedded Networked Sensor Systems* (Virtual Event, Japan) (*SenSys '20*). Association for Computing Machinery, New York, NY, USA, 150–163.
- [37] Dong Li, Jialin Liu, Sunghoon Ivan Lee, and Jie Xiong. 2022. Lasense: Pushing the limits of fine-grained activity sensing using acoustic signals. *Proceedings of the ACM on Interactive, Mobile, Wearable and Ubiquitous Technologies* 6, 1 (2022), 1–27.
- [38] Xiaoxuan Liang, Zhao long Wei, Dong Li, Jie Xiong, and Jeremy Gummesson. 2024. SONDAR: Size and Shape Measurements Using Acoustic Imaging. In *Proceedings of the Twenty-fifth International Symposium on Theory, Algorithmic Foundations, and Protocol Design for Mobile Networks and Mobile Computing* (Athens, Greece) (*MobiHoc '24*). Association for Computing Machinery, New York, NY, USA, 361–370. doi:10.1145/3641512.3686359
- [39] Yumeng Liang, Anfu Zhou, Xinzhe Wen, Wei Huang, Pu Shi, Lingyu Pu, Huanhuan Zhang, and Huadong Ma. 2023. airBP: Monitor Your Blood Pressure with Millimeter-Wave in the Air. (22 11 2023), 1–32. doi:10.1145/3614439
- [40] Li-Jen Liao, Wu-Chia Lo, Wan-Lun Hsu, Po-Wen Cheng, and Cheng-Ping Wang. 2017. Assessment of pain score and specimen adequacy for ultrasound-guided fine-needle aspiration biopsy of thyroid nodules. *Journal of Pain Research* Volume 11 (Dec. 2017), 61–66. doi:10.2147/jpr.s148088
- [41] Yinji Ma, Jungil Choi, Aurélie Hourlier-Fargette, Yeguang Xue, Ha Uk Chung, Jong Yoon Lee, Xiufeng Wang, Zhaoqian Xie, Daeshik Kang, Heling Wang, Seungyong Han, Seung-Kyun Kang, Yisak Kang, Xinge Yu, Marvin J. Slepian, Milan S. Raj, Jeffrey B. Model, Xue Feng, Roozbeh Ghaffari, John A. Rogers, and Yonggang Huang. 2018. Relation between blood pressure and pulse wave velocity for human arteries. *Proceedings of the National Academy of Sciences* 115, 44 (Oct. 2018), 11144–11149. doi:10.1073/pnas.1814392115
- [42] Connor MacIsaac, Macros Nguyen, Alexander Uy, Tianmin Kong, and Ava Hedayatipour. 2025. A Programmable Gain Calibration Method to Mitigate Skin Tone Bias in PPG Sensors. *Biosensors* 15, 7 (July 2025), 423. doi:10.3390/bios15070423
- [43] Grace McConnochie, Aaron Fox, Heather Badger, Clint Bellenger, and Dominic Thewlis. 2025. Fatigue assessment in distance runners: A scoping review of inertial sensor-based biomechanical outcomes and their relation to fatigue markers and assessment conditions. *Gait & Posture* 115 (Jan. 2025), 21–33. doi:10.1016/j.gaitpost.2024.10.012
- [44] Medi-stats. [n. d.] Operating BP+. Online. <https://www.medi-stats.com/augmentation-index>
- [45] Alessandro Montanari, Ashok Thangarajan, Khaldoon Al-Naimi, Andrea Ferlini, Yang Liu, Ananta Narayanan Balaji, and Fahim Kawsar. 2024. OmniBuds: A Sensory Earable Platform for Advanced Bio-Sensing and On-Device Machine Learning. doi:10.48550/ARXIV.2410.04775
- [46] Wilmer W. Nichols, Michael O'Rourke, Charalambos Vlachopoulos, and Elazer R. Edelman. 2022. *McDonald's Blood Flow in Arteries: Theoretical, Experimental and Clinical Principles*. CRC Press. doi:10.1201/9781351253765
- [47] Jakob Nielsen and Thomas K. Landauer. 1993. A mathematical model of the finding of usability problems. In *Proceedings of the SIGCHI conference on Human factors in computing systems - CHI '93 (CHI '93)*. ACM Press, 206–213. doi:10.1145/169059.169166
- [48] Jens Nürnberger, Rene Michalski, Tobias R Türk, Anabelle Opazo Saez, Oliver Witzke, and Andreas Kribben. 2010. Can arterial stiffness parameters be measured in the sitting position? *Hypertension Research* 34, 2 (Oct. 2010), 202–208. doi:10.1038/hr.2010.196
- [49] Theodore G. Papaioannou, John Thymis, Dimitrios Benas, Helen Triantafyllidi, Gavriela Kostelli, George Pavlidis, Fotini Kousathana, Kostantinos Katogiannis, Dimitrios Vlastos, Vaia Lambadiari, Evangelia Papadavid, John Parissis, Dimitrios Tousoulis, and Ignatios Ikonomidis. 2019. Measurement of central augmentation index by three different methods and techniques: Agreement among Arteriograph, Complior, and Mobil-O-Graph devices. *The Journal of Clinical Hypertension* 21, 9 (Aug. 2019), 1386–1392. doi:10.1111/jch.13654
- [50] Kun Qian, Chenshu Wu, Fu Xiao, Yue Zheng, Yi Zhang, Zheng Yang, and Yunhao Liu. 2018. Acousticcardiogram: Monitoring Heartbeats using Acoustic Signals on Smart Devices. In *IEEE INFOCOM 2018 - IEEE Conference on Computer Communications*. 1574–1582.
- [51] Qualcomm Technologies Incorporated 2020. *Qualcomm Aqstic smart speaker amplifier*. Qualcomm Technologies Incorporated. <https://www.qualcomm.com/products/internet-of-things/consumer/audio/mobile-audio/wsa8815>
- [52] Margareta Ring, Maria Jolanta Eriksson, Juleen Rae Zierath, and Kenneth Caidahl. 2014. Arterial stiffness estimation in healthy subjects: a validation of oscillometric (Arteriograph) and tonometric (SphygmoCor) techniques. *Hypertension Research* 37, 11 (July 2014), 999–1007. doi:10.1038/hr.2014.115

- [53] Gregory A. et al. Roth. 2018. The Burden of Cardiovascular Diseases Among US States, 1990-2016. *JAMA Cardiology* 3, 5 (May 2018), 375. [doi:10.1001/jamacardio.2018.0385](https://doi.org/10.1001/jamacardio.2018.0385)
- [54] Tobias Röddiger, Michael Küttner, Philipp Lepold, Tobias King, Dennis Moschino, Oliver Bagge, Joseph A. Paradiso, Christopher Clarke, and Michael Beigl. 2025. OpenEarable 2.0: Open-Source Earphone Platform for Physiological Ear Sensing. *Proceedings of the ACM on Interactive, Mobile, Wearable and Ubiquitous Technologies* 9, 1 (March 2025), 1–33. [doi:10.1145/3712069](https://doi.org/10.1145/3712069)
- [55] Motohiro Shimizu and Kazuomi Kario. 2008. Review: Role of the augmentation index in hypertension. *Therapeutic Advances in Cardiovascular Disease* 2, 1 (Feb. 2008), 25–35. [doi:10.1177/1753944707086935](https://doi.org/10.1177/1753944707086935)
- [56] SphygmoCor. 2025. Vascular Biometric Monitor. <https://cardiex.com/>
- [57] Texas Instruments Incorporated 2018. TAS2562. Texas Instruments Incorporated. <https://www.ti.com/product/TAS2562>
- [58] Chuyu Wang, Lei Xie, Wei Wang, Yingying Chen, Yanling Bu, and Sanglu Lu. 2018. RF-ECG: Heart Rate Variability Assessment Based on COTS RFID Tag Array. *Proceedings of the ACM on Interactive, Mobile, Wearable and Ubiquitous Technologies* 2, 2 (July 2018), 1–26. [doi:10.1145/3214288](https://doi.org/10.1145/3214288)
- [59] Wei Wang, Alex X. Liu, and Ke Sun. 2016. Device-Free Gesture Tracking Using Acoustic Signals. In *Proceedings of the 22nd Annual International Conference on Mobile Computing and Networking* (New York City, New York) (*MobiCom ’16*). Association for Computing Machinery, New York, NY, USA, 82–94. <https://doi.org/10.1145/2973750.2973764>
- [60] Nicolaas Westerhof, Nikolaos Stergiopoulos, Mark I.M. Noble, and Berend E. Westerhof. 2019. *Snapshots of Hemodynamics: An Aid for Clinical Research and Graduate Education*. Springer International Publishing. [doi:10.1007/978-3-319-91932-4](https://doi.org/10.1007/978-3-319-91932-4)
- [61] WHO. 2024. Cardiovascular diseases. online. https://www.who.int/health-topics/cardiovascular-diseases#tab=tab_1
- [62] Akira YAMASHINA, Hiroyumi TOMIYAMA, Tomio ARAI, Ken-ichi HIROSE, Yutaka KOJI, Yoji HIRAYAMA, Yoshio YAMAMOTO, and Saburoh HORI. 2003. Brachial-Ankle Pulse Wave Velocity as a Marker of Atherosclerotic Vascular Damage and Cardiovascular Risk. *Hypertension Research* 26, 8 (2003), 615–622. [doi:10.1291/hypres.26.615](https://doi.org/10.1291/hypres.26.615)
- [63] Akira YAMASHINA, Hiroyumi TOMIYAMA, Kazuhiko TAKEDA, Hideichi TSUDA, Tomio ARAI, Kenichi HIROSE, Yutaka KOJI, Saburoh HORI, and Yoshio YAMAMOTO. 2002. Validity, Reproducibility, and Clinical Significance of Noninvasive Brachial-Ankle Pulse Wave Velocity Measurement. *Hypertension Research* 25, 3 (2002), 359–364. [doi:10.1291/hypres.25.359](https://doi.org/10.1291/hypres.25.359)
- [64] Bin-Bin Zhang, Dongheng Zhang, Yadong Li, Zhi Lu, Jinbo Chen, Haoyu Wang, Fang Zhou, Yu Pu, Yang Hu, Li-Kun Ma, Qibin Sun, and Yan Chen. 2024. Monitoring long-term cardiac activity with contactless radio frequency signals. *Nature Communications* 15, 1 (Dec. 2024). [doi:10.1038/s41467-024-55061-9](https://doi.org/10.1038/s41467-024-55061-9)
- [65] Fusang Zhang, Zhi Wang, Beihong Jin, Jie Xiong, and Daqing Zhang. 2020. Your Smart Speaker Can “Hear” Your Heartbeat! *Proceedings of the ACM on Interactive, Mobile, Wearable and Ubiquitous Technologies* 4, 4 (Dec. 2020), 1–24. [doi:10.1145/3432237](https://doi.org/10.1145/3432237)
- [66] Qian Zhang, Dong Wang, Run Zhao, and Yinggang Yu. 2021. SoundLip: Enabling Word and Sentence-level Lip Interaction for Smart Devices. (30 3 2021), 1–28. <https://doi.org/10.1145/3448087>
- [67] Zhiyuan Zhao, Fan Li, Yadong Xie, Huanran Xie, Kerui Zhang, Li Zhang, and Yu Wang. 2024. HearBP: Hear Your Blood Pressure via In-ear Acoustic Sensing Based on Heart Sounds. *IEEE INFOCOM 2024 - IEEE Conference on Computer Communications*, 991–1000. [doi:10.1109/INFOCOM52122.2024.10621249](https://doi.org/10.1109/INFOCOM52122.2024.10621249)
- [68] Zixin Zheng, Yumeng Liang, Rui Lyu, Junjie Bao, Yiwen Huang, Anfu Zhou, Huadong Ma, Jingjia Wang, Xiangbin Meng, Chunli Shao, Yida Tang, and Qian Zhang. 2024. BP3: Improving Cuff-less Blood Pressure Monitoring Performance by Fusing mmWave Pulse Wave Sensing and Physiological Factors. In *Proceedings of the 22nd ACM Conference on Embedded Networked Sensor Systems* (Hangzhou, China) (*SenSys ’24*). Association for Computing Machinery, New York, NY, USA, 730–743. [doi:10.1145/3666025.3699370](https://doi.org/10.1145/3666025.3699370)

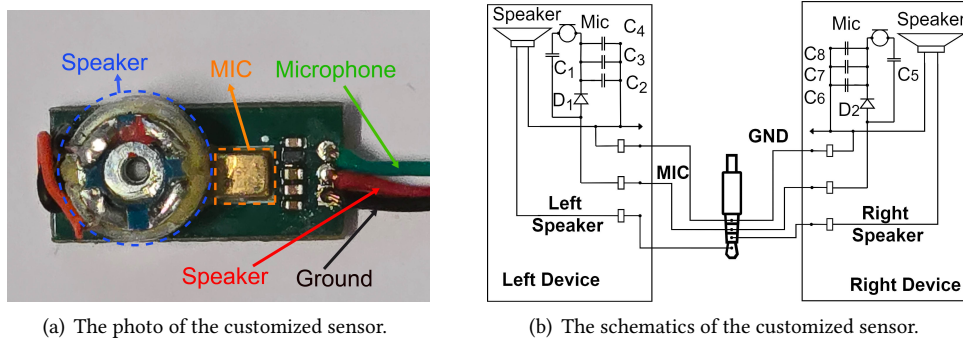


Fig. 18. Illustration of our customized sensor design. (a) The photo of the assembled sensor, showing the integrated speaker and microphone on a compact PCB. (b) The circuit schematic of the customized sensor, where two identical boards (left and right) are connected via a shared microphone input and ground through a 3.5mm TRRS jack.

A Custom Sensor Hardware Design

A.1 Hardware Design

To streamline assembly and enable large-scale deployment, we designed a low-cost, earphone-style sensor. As shown in Fig. 18(a), each customized printed circuit board (PCB) integrates a speaker and a microphone that are widely used in commodity earphones. When two boards are connected via an audio splitter, our system supports synchronized acquisition of reflected signals from two arterial sites.

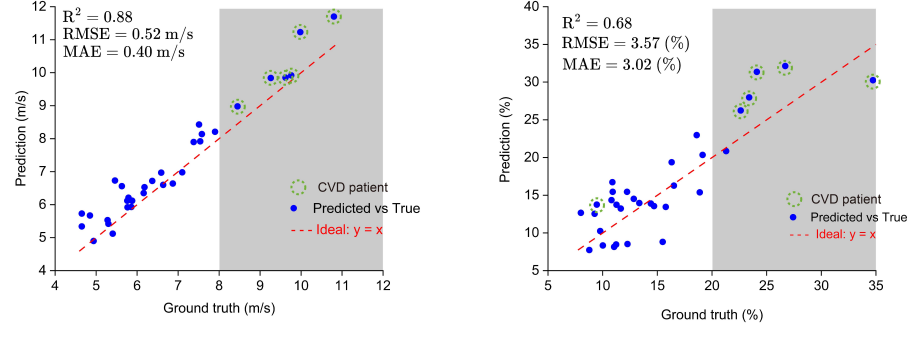
Fig. 18(b) presents the circuit schematic of our custom sensor. Similar to our commodity earphone prototype, we employ the TRRS (Tip-Ring-Ring-Sleeve) headphone interface standard, which provides four channels: left audio, right audio, microphone, and ground. Each PCB implements a single speaker channel—one using the left channel and the other the right—while both share a common microphone input.

The TRRS interface is traditionally intended for condenser microphones, which operate by superimposing an AC audio signal onto a DC-biased line. In contrast, our system incorporates MEMS microphones equipped with built-in preamplifiers, which require a stable DC power supply and output audio via a separate signal pin. Consequently, integrating these microphones with the TRRS socket necessitates a signal adaptation circuit.

Directly connecting the MEMS microphone output to the TRRS microphone line is infeasible due to signal interference on the DC-biased line. We address this challenge by interpreting it as an energy harvesting problem. As depicted in Fig. 18(b), we implement a simple rectification and filtering circuit using a diode (D1) and two $4.7\ \mu\text{F}$ capacitors (C2, C3), forming a passive energy harvester. The diode serves as a rectifier, while the capacitors function as low-pass filters. Additional components, including a bypass capacitor (C4) and a DC-blocking capacitor (C1), are incorporated in accordance with the MEMS microphone datasheet recommendations.

A $10\ \text{nF}$ decoupling capacitor (C1) is used to isolate the AC signal from the DC bias, ensuring clean signal transmission from the microphone. To suppress noise, a diode (RB161OS-40T18R) is placed at the microphone's V_{DD} terminal, preventing unwanted voltage fluctuations from feeding back into the smartphone. Additionally, capacitors C2 and C3 are connected in parallel across the microphone terminals to stabilize low-frequency voltage variations and absorb transient currents. A smaller capacitor (C4) is included to filter high-frequency noise sources such as RF interference and switching power supply noise.

A.2 The result of custom device



(a) The estimation PWV vs the ground truth.

(b) The estimation AIx vs the ground truth.

Fig. 19. An illustration of PWV and AIx measurements using the custom device compared to ground truth. The PWV higher than 8 m/s (highlighted in gray) or the AIx higher than 20% indicates the higher likelihood of cardiovascular diseases [5, 29].

As shown in Fig. 19, we used our custom device to measure the same 32 individuals in order to compare its performance with that of commodity earphones. The custom device reduced the mean absolute error (MAE) in PWV estimation from 0.47 m/s to 0.40 m/s and in AIx estimation from 3.23% to 3.02%. These results indicate that the custom device outperforms commodity earphones, likely due to its higher signal-to-noise ratio (SNR) and improved skin contact.

Received 1 May 2025; Revised 1 August 2025; Accepted 18 September 2025